Universitetet i Stavanger

FACULTY OF SCIENCE AND TECHNOLOGY

MASTER'S THESIS

Study program/Specialization: Petroleum Engineering/ Reservoir Engineering	Spring semester, 2018 Open
Author: Citra Kirana Lestari Nainggolan	…… (signature of author)
Supervisors: Pål Østebø Andersen, Dag Chun Standnes	
Title of master's thesis: **Core Flooding for Analysis of Capillary End Effect and Multiphase Flow Properties**	
Credits (ECTS): 30	
Keywords: Capillary end effect Capillary pressure Relative permeability Steady state condition Wettability alteration Experimental design	Number of pages: 77 +enclosure : N/A Stavanger, 16 July 2018

Core Flooding for Analysis of Capillary End Effect and Multiphase Flow Properties

---

Master thesis by

Citra Kirana Lestari Nainggolan (238183)

Spring 2018

FACULTY OF SCIENCE AND TECHNOLOGY

UNIVERSITY OF STAVANGER

Acknowledgement

This thesis would not have been completed without guidance, help, assistance and support from many individuals. Therefore, I would like to express my gratitude and appreciation to all those who gave me the possibility to finish my thesis.

I would sincerely like to thank my supervisors, Pål Østebø Andersen and Dag Chun Standnes for the patience, the support and the excellent guidance of my research, and for the knowledge, from the start until the final process of finishing my thesis, so that I can develop the understanding of the topic of my thesis. It is a pleasure to work together with you.

My special thanks to Kenny Walrond who helped and assisted me in the laboratory starting from preparing the setup until the final works. Thank you for always helping and answering our questions. Thank you for making us understand the equipment and the procedure in the laboratory.

I also want to thank Reza Askarinezhad who helped us during the wettability alteration process. Thank you for always answering our questions and thank you for providing us with the Quilon-L. My sincere thanks also go to Ola Ketil Siqveland, Kim Andre Nesse Vorland, and Reidar Inge Korsnes who gave us a solution when we encountered problems related to the equipment in the laboratory, especially Ola, thank you for letting us use your laboratory an for letting use the separator. I also want to thank Inger Olsen and Per Eirik Widvey who helped us with the procurement of the chemicals and the spare parts that we need in the laboratory. Thank you to Jorunn Vrålstad who helped us with the effluent test. I also want to thank you Aly Hamouda for providing the core material.

Thanks to my labmate, Eliana who have always been together with me during the experiment. Also, thank you to my friends especially my Indonesian friends. Without them, Stavanger will be boring. Thank you for always supporting me especially Kongs family.

Next, special gratitude to my family, Mama Naniek, Bang Leon and Bang Gindo for supporting me throughout my study and my life in general.

Lastly, thank you for the financial support from Indonesia Endowment Fund for Education (LPDP). Thus, my biggest appreciation to all people who manage the LPDP.

Abstract

The non-uniform saturations along the core is called capillary end effect. The capillary end effect is caused by the condition that the capillary pressure is zero outside the core. The presence of capillary end effect is significant in the laboratory. The determination of relative permeability and capillary pressure curves are much affected by capillary end effect. Capillary end effect influences the determination of end point saturation (residual oil saturation). The objective of this thesis is to estimate relative permeability and capillary pressure curves from the experiment to get a better understanding on capillary end effect by performing wettability alteration on the core samples that initially strong water-wet, spontaneous imbibition, forced imbibition(water-flooding), simulation of the experiment using simulator SENDRA, and sensitivity using simulator SENDRA. Wettability alteration is performed to change the wettability from water-wet to more oil-wet since capillary end effect is significant in more oil-wet state at water-flooding. Spontaneous imbibition is conducted to have a core system which has water saturation at P_c equal to zero. Forced imbibition is done by applying several rates to the core until it reaches a steady-state condition. Steady-state is reached when oil is perfectly immobilised due to entrapment, and the rate of injected water is equal to the rate of produced water (Virnovsky et al., 1995; Andersen et al., 2017). Cumulative oil and the differential pressure is measureed to estimate the relative permeability and capillary pressure curves by using simulator SENDRA. By conducting sensitivity in SENDRA, the main parameters that have a significant impact on capillary end effect are wettability, absolute permeability, rate, water viscosity and length of the core.

Keywords: Capillary end effect, Capillary pressure, Relative permeability, Steady state condition, Wettability alteration, Experimental design

Table of Contents

List of Figures

List of tables

Nomenclature

A	Cross-section area of core [cm^2]
a_o	Constant for imbibition curve from S_{wi} to S_{or} to define the negative part of the curve
a_w	Constant for imbibition curve from S_{wi} to S_{or} to define the positive part of the curve
c_o	Constant for imbibition curve from S_{wi} to S_{or} to define the negative part of the curve
c_w	Constant for imbibition curve from S_{wi} to S_{or} to define the positive part of the curve
D	Diameter of the core [cm]
f_w	Fractional flow function
$J(S_w)$	Leverett J-function scaling
K	Absolute permeability of core [Darcy]
k_{eff}	Effective permeability [Darcy]
k_r	Relative permeability
k_{rw}^0	Relative permeability of water at residual oil saturation (S_{or})
k_{ro}^0	Relative permeability of oil at initial water saturation (S_{wi})
L	Length of the core [cm]
m_d	Weight of dry core [g]
m_s	Weight of saturated core [g]
m_t	Weight of target core [g]
P	Pressure
P_{nw}	Pressure of the nonwetting
PV	Pore volume of the core
P_w	Pressure of the wetting phase
Q	Flow rate [mL/s]
R	Radius of the pore
S	Saturation
S_{or}	Residual oil saturation
S_w^*	Normalized water saturation
S_{wi}	Irreducible water saturation
S_w^{max}	Maximum saturation from the known injected rate
u_i	Darcy velocity
V_{bulk}	Bulk volume of the core
v_T	Interstitial Velocity

x	Position along the core

Greek

∂	partial derivative
ϕ	Porosity
ρ	Density
σ	Interfacial tension between two phases
θ	Contact angle measured through the wetting phase
μ	Viscosity of fluid [cp]
λ	Phase mobility

Indices

c	Capillary
i	Phase Index
w	Phase property water
o	Phase property oil
T	total

Abbreviation

EOR	Enhanced oil recovery

1 Introduction

1.1 Background

Energy is the basic need of human being. Growth in the world's population leads to increasing energy demand. Today, oil is still the world's dominant source of energy even though the renewable energy in global is growing. The oil industry is a high-risk and high-cost industry. The system is complicated, and everything should be calculated carefully. Reservoir simulation is used to predict reservoir performance over time. For a new field, simulation studies help to decide how many wells that should be drilled, type of artificial lift that should be used, surface facilities that should be developed, and the expected production of oil, water, and gas. For a developed field, simulation studies can give guidance to improve oil recovery by several the methods such as infill drilling, enhanced oil recovery (EOR) methods, and hydraulic fracturing. Many data are required as inputs in reservoir simulation. These are reservoir rock and fluid characterisation, well history, production history, and a reliable history matching to validate and modify the inputs. One of the critical aspects of reservoir rock characterisation is multiphase flow properties which cover which cover fluid saturation over time that are determined by capillary pressure and relative permeability. These properties are determined by carrying out a laboratory experiment on the cores from the reservoir.

Core flooding experiment is a standard test in the laboratory that is conducted to measure absolute permeability, relative permeability, saturation transition, and fractional flow. The computation of residual oil saturation is essential in reservoir simulation, especially for enhanced oil recovery procedure. The determination of relative permeability and capillary pressure curves are much affected by capillary end effect. Capillary end effect can cause a non-uniform saturation distribution along the core. However, in some cases, it is neglected (i.e. Buckley and Leverett (1942) neglected capillary effects (pressure of two phases are equal) to determine saturation distribution).

Capillary pressure exists because there are several phases inside the porous medium. Capillary pressure (P_c) is a factor that controls the fluid distribution of the reservoir rock. The presence of capillary end effect in the laboratory is significant due to the low permeable medium, it has a high value, while in open space it has a zero value. Due to the length and the boundary of the core, the core sample has discontinuity saturation profile along the core, and this phenomenon is called capillary-end effect.

Several studies about capillary end effect have been conducted. Virnovsky et al. (1995) determined the relative permeability and capillary pressure from steady-state flow experiments by varying the total rate and injected phase fraction. Abeysinghe et al. (2012) performed water-flood and oil-flood to water-wet and mix-wet cores. It is concluded that capillary end effect is dominant in water-flood of the mixed-wet case. Gupta and Maloney (2016) corrected the steady-state saturation and pressure drops by using the intercept model. They assumed that the pressure drop is fixed at a specific fractional flow if the capillary end effect region is less significant than the length of the core. Rapoport and Leas (1953) derived a scaling factor $Lu_T\mu_w$ as the parameters that are affecting capillary end effect, where L is the length of the core, u_T is the injection rate, and μ_w is the water viscosity. They stated that capillary end effect can be minimised by making that scaling factor high enough. Hadley and Handy (1956) derived a pressure profile equation due capillary end effect that including Rapoport Lea numbers and Engelberberts-Kliknkenberg number. Huang and Honarpour (1998) used the Corey-Burdine equations to make a correction in relative permeability and saturation calculation due to capillary end effect. Andersen et al. (2017) derived an explicit expression of average saturation, pressure drop, and estimated water relative permeability end point as a function of capillary number and saturation function shape parameter.

The difference between this study and the previous studies is that the lowest rate is applied to the core to capture capillary end effect on the low rate which is time consuming. The same assumptions as Virnovsky et al. (1995) and Andersen et al. (2017) are used in the experiment where single phase(brine) is injected to the core. The rate might be increased when the steady-state condition is reached.

1.2 Thesis Objective

The objectives of this thesis are:

1. To create an experimental system in the core in which measuring the capillary end effect in water-flooding is possible to perform by changing the wettability of the core from strong water-wet to be more oil-wet.
2. To estimate relative permeability and capillary pressure curves from the experiment.
3. To perform history matching of the experimental result by using SENDRA simulator and do sensitivity towards the model to determine the factors that affect the system and the experimental setup.

1.3 Method

The aim of this thesis is investigating the end effect of core flooding on four different cores with different wettability. The work is based on a laboratory experiment, but simple simulation using SENDRA is also conducted to estimate flow functions by history matching. Berea and Bentheimer core are used throughout this experiment. The initial wetting phase of the two cores is changed from strongly water-wet to more oil-wet for by using Quilon-L in DI water solution and mix-wet by using Quilon-L in n-decane solution. The cores are later saturated with brine. The initial water saturation is assumed small enough, and no water is produced while injecting other fluid. Then, the core is saturated with oil. Spontaneous imbibition is conducted as the next step. The primary procedure is forced imbibition by displacing oil by water in steady state condition. The term steady state in this thesis means fluid is produced with the same injection rate. Saturation function over time is recorded, and the correlation between capillary pressure and saturation is estimated by using the equation and history matching of experimental data.

1.4 Outlines

In the thesis, there are seven chapters to cover the work. The current section gives the background and the objectives of the thesis. Chapter 2 provides the fundamental theories related to the thesis topic. Chapter 3 gives a brief explanation about SENDRA simulator and the equation that will be used in the simulator. Chapter 4 presented the laboratory work details from the preparation of material, and equipment and the main experiment itself. Chapter 5 gives the result of laboratory work and the discussion about the result. Chapter 6 shows the history matching in SENDRA and sensitivity analysis on the parameters that might affect capillary end effect. The last chapter concludes the comprehensive study and recommendations for future research.

2 Fundamental Theories

2.1 Capillary Pressure

Capillary pressure is a factor that controls the fluid distribution (saturation and saturation history) of the reservoir rock. The combination between the surface and interfacial tensions of the rock and fluids results in the capillary forces in the reservoir (Ahmed, 2001). Capillary pressure is the pressure difference between two immiscible fluids that are in contact. Capillary pressure can be calculated by equation (1).

$$P_c = P_{nw} - P_w \tag{1}$$

Where P_c is capillary pressure, P_{nw} is the pressure of the nonwetting phase, and P_w is the pressure of the wetting phase.

Young Laplace equation for the capillary rise in a tube is expressed by equation (2) :

$$P_c = \frac{2\sigma cos\theta}{R} \tag{2}$$

Where σ is interfacial tension between two phases, θ is contact angle measured through the wetting phase, and R is the radius of the pore.

Based on equation (1) and (2), capillary pressure is affected by the interfacial tension of the fluid, the wettability of the rock, and pore size (Green and Willhite 1998). The value of capillary pressure can be positive or negative. Figure 5 shows the typical capillary pressure curve for oil and water system. A capillary pressure either follows increasing wetting phase saturation(imbibition) or decreasing wetting phase saturation(drainage).

- Drainage process is the displacement of wetting phase (brine) by non-wetting phase (oil). In this case, the wetting phase(brine) saturation is decreasing. A negative value of capillary pressure describes spontaneous drainage, while the positive value of it describe forced drainage. Primary drainage is started from initial water saturation 100% and then decreasing water saturation.
- Imbibition process is the displacement of non-wetting phase (oil) by wetting phase(brine). In this case, the wetting phase(brine) saturation is increasing. A positive value of capillary pressure describes spontaneous imbibition, while a negative value of it describe forced imbibition.

This thesis focuses on the imbibition process, spontaneous imbibition and forced imbibition. Water saturation at capillary pressure is equal to zero is obtained from spontaneous imbibition.

Moreover, by performing forced imbibition, displacement pressure and fluid saturation are recorded to identify capillary pressure end effect (negative part of capillary pressure curve). The saturation point from forced imbibition is crucial. This point is measured based on the applied rate or pressure in the core holder. If the pump system in the laboratory is is high enough, corrected residual oil saturation that is needed in a simulation procedure can also be measured.

2.2 Wettability

Wettability is one of the critical parameters of the reservoir rock, primarily to determine the EOR method. The definition of wettability is the measure of the tendency of one of the fluids to attach to the surface of the porous medium in the presence of the other fluid (Donaldson and Alam 2008). The component of oil, brine, rocks, and the interactions between those components affect the wettability. Wettability is an essential aspect on capillary end effect. It determines the interval between the saturation at the outlet (P_c=0) and the residual oil saturation. The end effect is significant when this interval is large enough (away from (1-S_{or}) and closer to S_w when capillary pressure is equal to zero).

2.2.1 Wettability measurement

In this thesis, the wettability is measured by using spontaneous imbibition method at room temperature. The flow rate of wetting fluid (in this case brine) spontaneously imbibed into a core and replacing the non-wetting fluid (in this case oil) by the action of capillary forces is measured (Honarpour et al., 1986). The detail of the spontaneous imbibition cell is described in chapter 4.3.5.

2.2.2 Wettability classification

Wettability can be classified as a range from strongly water-wet to strongly oil-wet. The rock can be classified as preferentially water-wet if the reservoir has preference for water and the contact angle between water and rock surface is less than 90°. Preferentially oil-wet if the reservoir has preference for oil and the contact angle is greater 90°. Neutral or intermediate wettability if there is no preference of the rock towards oil or water. Fractional-wettability where the preferential wetting distributes randomly throughout the rock. The term mixed wettability was first mentioned by Salathiel (1973), in this condition, the small pores and grains have preference for water, and the surfaces of the larger pores have a preference to oil and have a continuous phase of oil.

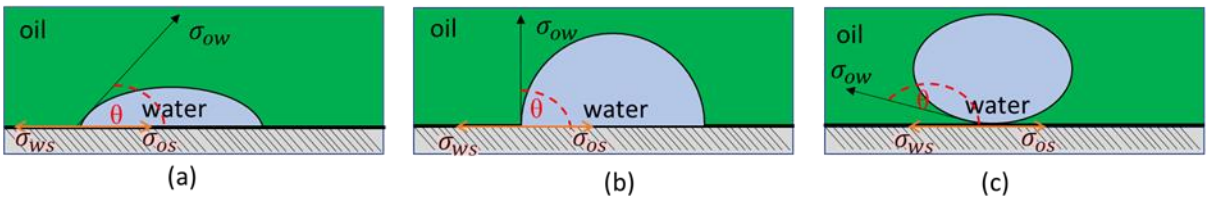

Figure 1. Contact angle wettability illustration for the oil-water system. (a) water-wet; (b) neutral-wet; (c) oil-wet.

In this thesis, the wettability of sandstone core is changed from strongly water-wet to mixed-wet core and oil-wet core to investigate capillary end effect.

2.3 Permeability

2.3.1 Absolute permeability

The ability of the formation to transport fluid is described as permeability. By using Darcy's equation for horizontal flooding, absolute permeability can be expressed as:

$$K = -\frac{Q\mu L}{\Delta P A} \tag{3}$$

Where K is the absolute permeability of core [Darcy], Q is the flow rate [mL/s], μ is the viscosity of fluid [cp], L is the length of the core [cm], A is the cross-section area of core [cm^2], and ΔP is the differential pressure across the core [atm].

2.3.2 Relative Permeability

In multiphase flow, relative permeability can be described as the ratio between the effective permeability of each phase to absolute permeability. There are two methods to measure the relative permeability either steady-state and unsteady state. The steady-state method takes more time than the unsteady-state method, but the unsteady-state method is more complicated to solve mathematically (Honarpour et al., 1986). Both methods can be used, and it should give the same value.

$$k_{ri} = \frac{k_{effi}}{K}, i = w, 0 \tag{4}$$

Where K is absolute permeability, k_r is relative permeability, and k_{effi} is effective permeability. Index $i = w, 0$ represent phase properties water and oil. This thesis focus on oil and water system in which relative permeability is usually plotted as a function of water saturation.

Figure 2 illustrates typical relative permeability curves. The value of relative permeability is between zero and one as a ratio. Water saturation value is also between zero and one as a fraction. When producing oil, the relative permeability of oil decreases and the relative permeability of water increases as the water saturation increases. The highest value of relative permeability of water is reached when the water saturation is equal to one minus residual oil saturation (S_{or}) as no more oil can be produced.

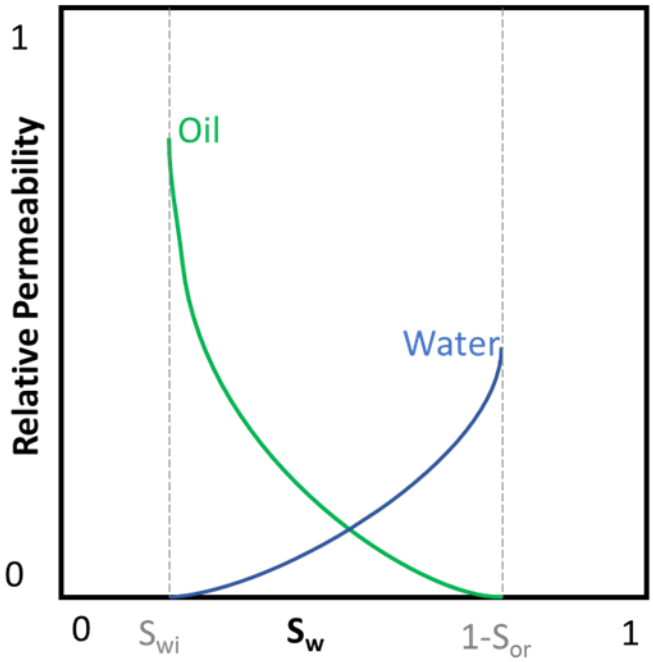

Figure 2. Relative permeability oil-water system curves.

2.4 Capillary End Effect

Hadley and Handy (1956) described capillary end effect as the holdup of the preferentially wetting phase at the outlet of the porous medium during fluid flow. Figure 3 illustrates the capillary end effect. Water is injected from x=∞ in the negative direction with a known rate u_T. The blue area indicates the water saturation at zero capillary pressure. The blue line shows the saturation distribution along the core due to the capillary end effect. If there is no capillary end effect, then the blue line will be a straight line. $S_w^{max}$is the maximum saturation from the known injected rate (u_T), the value is depend on the injection rate.

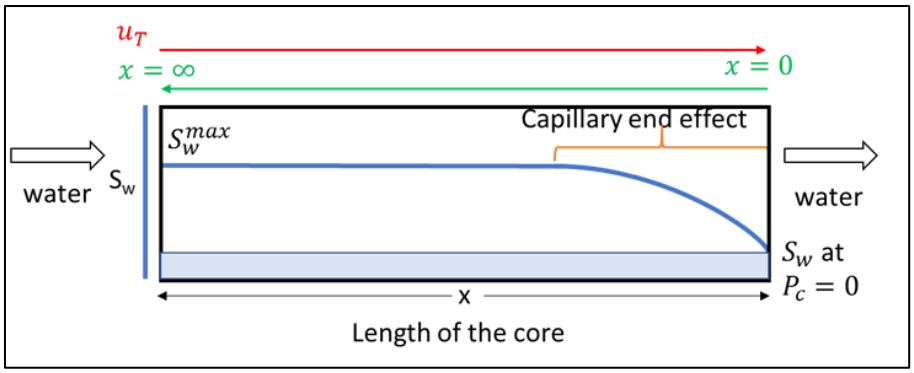

Figure 3. Illustration of the capillary end effect.

The steady-state end effect is the focus of this thesis. The core flooding experiment is executed by continuously injecting brine to replace oil through the core. Steady-state is reached when oil is perfectly immobilised due to entrapment, and the rate of injected water is equal to the rate of produced water (Virnovsky et al., 1995; Andersen et al., 2017). Figure 4 shows the experimental procedure where brine is injected into the core with several steps of the rate under the steady condition, following the procedure from Virnovsky et al. (1995). The dashed line in illustrates the steady state condition where oil is immobilised, the saturation does not change with time, and the amount of water injection is equal to water production. Most oil is produced at the initial rate.

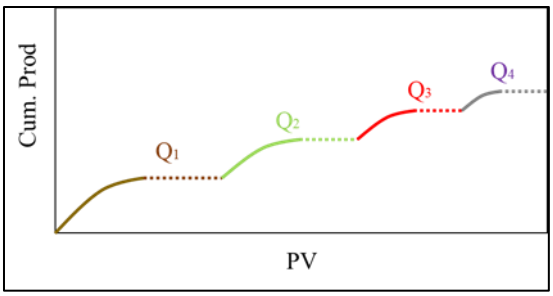

Figure 4. Illustration of core flooding experiment and a steady-state condition.

2.4.1 Mathematical model

The mathematical model in this thesis is based on Andersen et al. (2017) for one dimensional, two-phase immiscible flow of oil (o) and water (w), and incompressible fluids in a porous medium.

Darcy's law:

$$u_i = -K\lambda_i \frac{\partial P_i}{\partial x}, \quad \lambda_i = \frac{k_{ri}}{\mu_i}, \ \lambda_T = \lambda_o + \lambda_w \quad (i = o, w) \tag{5}$$

Conservation of mass gives

$$\frac{\partial u_i}{\partial x} + \phi \frac{\partial S_i}{\partial t} = 0, \qquad (i = o, w) \tag{6}$$

Where u_i is darcy velocity, K absolute permeability, P_i pressure, k_{ri} relative permeability, μ_i viscosity and $S_i$saturation. Index $i = o, w$ represent phase properties. In this case, gravity effect is neglected.

The pressures are related by the capillary pressure function $P_c = P_o - P_w$. u_T is the total flux from equation (5) for oil and water phase, and can be expressed as

$$u_T = u_w + u_o = -K\lambda_w \frac{\partial P_w}{\partial x} - K\lambda_o \frac{\partial P_o}{\partial x} = -K(\lambda_T - \lambda_o) \frac{\partial P_w}{\partial x} - K\lambda_o \frac{\partial P_o}{\partial x}$$

$$u_T = -K\lambda_o \frac{\partial (P_o - P_w)}{\partial x} - K\lambda_T \frac{\partial P_w}{\partial x}$$

$$u_T = -K\lambda_o \frac{\partial P_c}{\partial x} - K\lambda_T \frac{\partial P_w}{\partial x} \tag{7}$$

By using constraint $S_o + S_w = 1$, and adding the transport equation (6) implies that

$$\frac{\partial u_T}{\partial x} + \phi \frac{\partial (S_w + S_w)}{\partial t} = 0,$$

$$\frac{\partial u_T}{\partial x} = 0 \tag{8}$$

u_T is constant along the x-axis, however, it can be changed at any time along the x-axis. From equation (7), $\frac{\partial P_w}{\partial x}$ is given by

$$K\lambda_T \frac{\partial P_w}{\partial x} = -u_T - K\lambda_o \frac{\partial P_c}{\partial x}$$

$$\frac{\partial P_w}{\partial x} = -\left(\frac{u_T + K\lambda_o \frac{\partial P_c}{\partial x}}{K\lambda_T} \right) \tag{9}$$

Mass balance of water phase can be expressed as

$$\phi \frac{\partial S_w}{\partial t} = -\frac{\partial u_w}{\partial x} \tag{10}$$

By inserting equation (9), the mass balance of water phase (10) can be written as

$$\phi \frac{\partial S_w}{\partial t} = -\frac{\partial}{\partial x}\left(-K\lambda_w \frac{\partial P_w}{\partial x}\right)$$

$$\phi \frac{\partial S_w}{\partial t} = \frac{\partial}{\partial x}\left(-f_w u_T - K f_w \lambda_o \frac{\partial P_c}{\partial x}\right) \quad (11)$$

Where f_w is the fractional flow function.

$$f_w = \frac{\lambda_w}{\lambda_T} = \frac{\lambda_w}{\lambda_w + \lambda_o} \quad (12)$$

In (Buckley & Leverett, 1942) equation, it is assumed that capillary pressure is neglected. Therefore, equation (11) can be written as

$$\phi \frac{\partial S_w}{\partial t} = -u_T \frac{\partial}{\partial x}(f_w) \quad (13)$$

However, in thesis capillary pressure is investigated and equation (11) is used together with the initial and the boundary conditions.

2.4.1.1 Boundary conditions

Andersen et al. (2017) mentioned that the brine is assumed to be injected from $x = \infty$ in the negative direction, i.e. u_T (< 0) is known and equal to u_w, since only water flows in the direction towards the outlet at the inlet. The boundary condition can be seen from Figure 3.

$$f_w(x = \infty) = 1, \qquad \left.\frac{\partial P_c}{\partial x}\right|_{x=\infty} = 0 \quad (14)$$

Zero capillary pressure is defined as the boundary at the outlet, and this defines the capillary effect.

$$P_c|_{x=0} = 0 \quad (15)$$

2.4.1.2 Steady-state

As explained by Andersen et al. (2017), there is no saturation and pressure changes with time in steady state condition:

$$\partial_t S_i = 0, \qquad \partial_t P_i = 0\,, \qquad (i = o, w) \quad (16)$$

By inserting steady-state equation (16) into the mass balance of water phase (11), then water saturation as a function of spatial coordinate ($S_w = S_w(x)$) can be written as:

$$0 = \frac{\partial}{\partial x}\left(-f_w u_T - K f_w \lambda_o \frac{\partial P_c}{\partial x}\right) \quad (17)$$

By doing the integration of equation (17) and the boundary conditions thus give:

$$0 = \left(-f_w u_T - K f_w \lambda_o \frac{\partial P_c}{\partial x}\right)\Big|_x - \left(-f_w u_T - K f_w \lambda_o \frac{\partial P_c}{\partial x}\right)\Big|_{x=\infty}$$

$$u_T = f_w u_T + K f_w \lambda_o \frac{\partial P_c}{\partial x} \tag{18}$$

By gathering variable u_T on the same side, equation (18) can be rewritten as:

$$u_T(1 - f_w) = K f_w \lambda_o \frac{\partial P_c}{\partial x}$$

$1 - f_w$ can be expressed as the fractional flow function of oil $\frac{\lambda_o}{\lambda_w + \lambda_o}$, then equation (18) can be rewritten as

$$u_T = K \lambda_w \frac{\partial P_c}{\partial x} \tag{19}$$

From the boundary condition, u_T (< 0) is known, λ_w and K are positive. That means $\frac{\partial P_c}{\partial x} = \frac{u_T}{K \lambda_w}$ will be negative. λ_w is a function of saturation (S_w). From equation (19), and using that $\frac{\partial P_c}{\partial x} = \frac{\partial P_c}{\partial S_w} \times \frac{\partial S_w}{\partial x}$, the saturation gradient along the core at steady-state can be written as:

$$\frac{\partial S_w}{\partial x} = \frac{u_T}{\lambda_w K \frac{\partial P_c}{\partial S_w}} \tag{20}$$

The value of the saturation gradient is positive. That means by increasing the saturation, $(1 - S_{or})$ can be obtained.

2.4.1.3 Leverett scaling

It is convenient to introduce dimensionless position x_D. Set $x_D = \frac{x}{L}$, where x is the position along the core and L is the length of the core, then

$$\frac{\partial S_w}{\partial x_D} = \frac{\partial S_w}{\partial x} \cdot \frac{\partial x}{\partial x_D} = \frac{\partial S_w}{\partial x} \cdot L \tag{21}$$

Capillary pressure is assumed following Leverett J-function scaling:

$$P_c = \sigma \sqrt{\frac{\phi}{K}} J(S_w) \tag{22}$$

Where σ is the interfacial tension between oil and water, and $J(S_w)$ is Leverett J-function scaling. Interstitial Velocity (v_T) can be expressed as

$$u_T = \phi v_T \tag{23}$$

Substitution on equation (20), the dimensionless saturation gradient along the core can be expressed as

$$\frac{\partial S_w}{\partial x_D} = \frac{L v_T}{\frac{k_{rw}}{\mu_w}\sigma\sqrt{\frac{K}{\phi}}\frac{\partial J(S_w)}{\partial S_w}} \tag{24}$$

High value of $\frac{\partial S_w}{\partial x_D}$ means that S_w quickly goes from S_w at P_c equal to zero to 1-S_{or}. Low value of $\frac{\partial S_w}{\partial x_D}$ means that S_w lies around S_w where P_c equal to zero and the end effect will become strong. Equation (24) shows the similar correlation as scaling factor $Lu_T\mu_w$ from Rapoport and Leas (1953). Capillary end effect can be minimized at long core, high rate, high viscosity of water, and low permeability.

2.4.2 Wettability on the capillary end effect

- From equation (20) that is built from the mathematical model by Andersen et al. (2017), capillary pressure along the spatial coordinate is affected by the fractional flow and the constant flux on steady-state condition. The result of a study from Abeysinghe et al. (2012) shows that at the water-wet condition, there is no rate dependency in water saturation distribution. At water-wet media, there is no difference between the value of P_c between saturation where P_c equal to zero and P_c at 1-S_{or}. Thus, at the water-wet system, it does not matter on saturation distribution how strong the capillary number is. While, at the mixed-wet condition, capillary end effect can be minimised by using the higher rate. From equation (20), the capillary end effect is significant when the low rate is applied.
- A study from Abeysinghe et al. (2012) mentioned that there is no holdup of oil during water injection into a water-wet core. Capillary pressure has positive and negative value for the water-wet system and oil-wet system. However, at the water-wet system, the negative part becomes minus infinite almost for the same saturation value where P_c equal to zero. At more oil-wet system, the negative part after P_c equal to zero varies along the saturation until 1-S_{or}. Spontaneous imbibition is displayed on the positive part of the curve, and force imbibition is displayed on the negative part of the curve. The difference in the wettability of the core can be seen from the value of water saturation after spontaneous imbibition. If the change of water saturation in spontaneous imbibition is small, the core is most likely oil-wet. On the other hand, if the change is significant, then the core is most likely water-wet.

3 Sendra Simulator

SENDRA is a core flooding simulator that is used to simulate and verify SCAL experiment (Lenormand et al., 2017). History matching is performed by using simulator SENDRA (version 2016.1). It covers the whole experiment process including the steady-state flow corresponding to the assumption in this experiment (constant rate).

3.1.1 Relative permeability curve fitting

In this thesis, Brooks and Corey (1964) equation is used for history matching.

$$k_{rw} = k_{rw}^{0}(S_w^*)^{N_w} \tag{25}$$

$$k_{ro} = k_{ro}^{0}(1 - S_w^*)^{N_o} \tag{26}$$

Where k_{rw}^{0} is the relative permeability of water at residual oil saturation (S_{or}), and k_{ro}^{0} is the relative permeability of oil at initial water saturation (S_{wi}).

The shape of water and oil relative permeability curve is attained by the parameter N_w or N_o. The curve that will be used in the simulation is constructed by changing these parameters and keeping the end point of saturation, S_{wi} and S_{or}.

The normalised water saturation can be calculated as:

$$S_w^* = \frac{S_w - S_{wi}}{1 - S_w - S_{or}} \tag{27}$$

Where S_w^* is the normalized water saturation, S_{wi} is the irreducible water saturation water saturation, and S_{or} is the residual oil saturation.

3.1.2 Two-phase capillary Pressure correlation

In this thesis, Skjaeveland et al. (2000) equation are used for history matching. Skjaeveland et al. (2000) generated a capillary pressure equation for a mixed-wet reservoir that comprises the imbibition as can be seen in Figure 5.

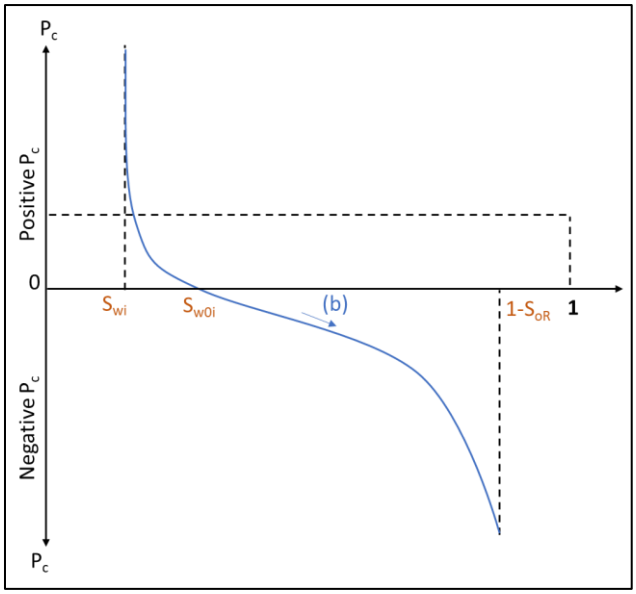

Figure 5. Schematic of bounding curves, capillary pressure Pc as a function of water saturation Sw: (b) imbibition. Redrawn from Skjaeveland et al. (2000).

The general expression for imbibition curve is expressed as

$$P_{ci} = \frac{c_w}{(\frac{S_w - S_{wi}}{1 - S_{wi}})^{a_w}} - \frac{c_o}{(\frac{1 - S_w - S_{or}}{1 - S_{or}})^{a_o}} \tag{28}$$

Where P_c is the capillary pressure [Pa], S_w is the water saturation [-], S_{wi} is the initial water saturation [-], and S_{or} is the residual oil saturation [-]. The $c_w, a_w, c_o,$ and a_o are constants for imbibition curve from S_{wi} to S_{or}. The value of $a_w,$ and c_w are used to define the positive term of the curve. While the value of $a_o,$ c_o are used to define the negative term of the curve. At S_{wi}, the negative term has $S_o = 1 - S_{wi}$ and the value is not zero. It means that both terms are needed to make a capillary pressure equal to zero whether the saturation point at capillary pressure equal to zero is at S_{wi} or any other saturation value.

4 Experimental Work

In this part, two types of the core material is used, Bentheimer and Berea. The cores are treated by using Quilon to change the wettability to be more oil-wet. Spontaneous imbibition is performed to get the water saturation at capillary pressure equal to zero. Next, water flooding is performed at a constant rate with rate increases in steps. Differential pressure and cumulative oil production versus time are recorded to provide the capillary pressure and relative permeability curves of the core.

4.1 Experimental Material

4.1.1 Core

Four cores are used in this experiment with two type of core materials, Berea and Bentheimer core plug. Frantz Jr. et al. (1993) that Berea sandstone is believed to have deposited in a shallow marine environment. The core is drilled from an outcrop in Ohio, United States. In the core flood experiment, the upper Berea sandstone unit is the most commonly used. The rock has well-sorted and well-rounded sand grains (Churcher et al., 1991). Bentheimer sandstone is a type of shallow marine deposition. This core is taken from an outcrop of Netherland and German border. Bentheimer is an ideal rock for experimental study due to its lateral continuity and homogeneous block-scale (Peksa et al., 2015). The Bentheimer cores were drilled from the same large block.

The main component on both Bentheimer and Berea is quartz (Peksa et al., 2015; Frantz Jr. et al., 1993). Therefore, initially, the cores have more preference on water. Table 1 gives the necessary physical core data of Berea and Bentheimer cores.

Table 1. Core Properties.

	Core Type			
Parameter	**Berea**	**Bentheimer_1**	**Bentheimer_2**	**Bentheimer_3**
Length (mm)	89.24	89.89	90.03	90.03
Diameter (mm)	37.72	37.79	37.81	37.74
ϕ (%)	20.89	22.89	21.79	21.82
K (Darcy)	0.63	3.20	3.00	3.10
Type	Sandstone	Sandstone	Sandstone	Sandstone

4.1.2 Fluid and Chemical

Table 2 shows the properties of fluids that are used in this experiment.

Table 2. Properties of fluids.

Liquid	Density at 20^{O}C(g/cm^{3})	Viscosity (cP)
NaCl 1 M	1.0386	1.09
NaCl 0.1 M	1.0019	1.01
Quilon-H (3% Weight) in n-decane	0.7386	-
Quilon-L (3% Weight) in n-decane	0.7388	-
Quilon-L (3% Weight) in distilled water	0.999	-
n-Decane	0.73	0.92

4.1.2.1 Brine

Sodium chloride (NaCl) 1 M and 0.1 M are used during the experiment. The liquid density is measured by using a densitometer Anton Paar model DMA 4100 M shown in Figure 7 at room temperature 20^{o}C. Firstly, the tube is cleaned with acetone. Next, the density is calibrated by using distilled water. The densitometer is considered valid if the measurement of distilled water has the same value as in the literature. Then, the density of brine is recorded by a densitometer. The measurement is done several times for accuracy. The viscosity of brine is determined based on the experiments by Kestin et al. (1981) at pressure 6.5 bar and room temperature 20^{o}C.

4.1.2.2 Quilon

In this thesis, Quilon is used to alter the wettability of the core. Quilon complexes are manufactured by Zaclon LLC. Quilon is a dark green solution, largely in isopropanol, of a chemically reactive compound in which a C14-1C18 fatty acid is coordinated with trivalent chromium. The fatty-acid group in the Quilon is hydrophobic (Quilon data sheet, 2018). Therefore, after a reaction with the core, it is oriented away from the surface to give the core its oil-wet characteristic.

Initially, the wettability alteration by using Quilon was proposed by (Tiffin & Yellig, 1983). He used Quilon-C to change the wettability of Berea from strongly water-wet to oil-wet, while Maini et al. (1986) used Quilon-S with some minor differences related to the grade of Quilon.

In this experiment, wettability alteration is based on a method which proposed by Abeysinghe et al. (2012). Initially, Quilon-H was used in the experiment with the assumption that the behaviour of Quilon-H is similar to Quilon-L. There is no study about the solubility of Quilon-

H in n-decane and distilled water. However, after performing the wettability alteration in this experiment. It is found that Quilon-H is not soluble in n-decane.

Therefore, in the end, Quilon-L is used to perform the wettability alteration on the core. Criollo (2011) observed that Quilon-L is soluble in both distilled water and n-decane. The differences between Quilon-C, S, H and L is the grade. Quilon-H and L are more concentrated than Quilon-C and S (Quilon data sheet, 2018). The more concentrated grade provide both economic and storage advantages. The fluid properties of Quilon-H and Quilon-L solution can be seen in Table 2.

4.1.2.3 Oil

N-decane is used as oil in the experiment. The chemical formula of decane is $CH_3(CH_2)_8CH_3$. From the physical appearance, the colour of n-decane is like water which is colourless with a density less than water ("PubChem Compound Database,"). Table 2 shows the properties of n-decane.

4.1.2.4 Sudan Blue GN

Distinguishing oil and brine inside the flow line is difficult. Therefore, for the Bentheimer_3 experiment, Sudan Blue GN is used for n-decane colouration. Sudan Blue GN is a blue-black powder that is soluble in n-decane but, not in water. It is manufactured by Waldeck GmbH & Co. KG, Division Chroma. The chemical formula of Sudan Blue GN is $C_{22}H_{18}N_2O_2$. Sudan blue GN is not reactive with the rock.

4.2 Experimental equipment

4.2.1 Quizix QX20K pump

The pump that is used during the experiment is QX20K. This pump is manufactured by Chandler Engineering. There are two cylinders to store and to pump fluid which have a total volume of 7 mL. These two cylinders make it possible to inject fluid continuously, by changing the cylinder simultaneously. The maximum cylinder pressure rating of 20,000 psi, the minimum of the flow rate of 0.0001 mL/min and a maximum flow rate of 7.5 mL/minute ("Quizix QX Series", 2018).

Figure 6. Quizix QX20K pump.

4.2.2 Anton Paar 4100 density meter

The density meter is manufactured by Anton Paar. This density meter can show 4-digit density value. In this thesis, the density meter is used to measure the density of the brine.

Figure 7. Anton Paar 4100 Density Meter.

4.2.3 Separator

Usually, burette is used to collect and measure the volume of the effluent. However, the volume of the burette is limited, and brine is injected continuously. In this experiment, the volume of burette is only 25 mL, while the fluid production is larger than 25 mL per day at a higher rate. Therefore, the separator was used in the force imbibition procedure where a higher rate was applied.

The separator that is used in this experiment makes use of the gravity effect where the fluid with lower density will stay on the top, and the fluid with higher density will stay in the bottom.

Figure 8 illustrates the schematic of the separator. The burette is placed upside down, and it is connected to a rubber line. Burette and the left section of the rubber line are initially filled with brine at the same fluid level, while the other rubber line is empty. The production fluid flow through the orange line from the core holder to the burette. When the fluid is produced, the oil will stay in the top part of the burette, while the brine will flow through the right section of rubber line to the effluent collector. By using this separator, oil and brine can be measured at the same time.

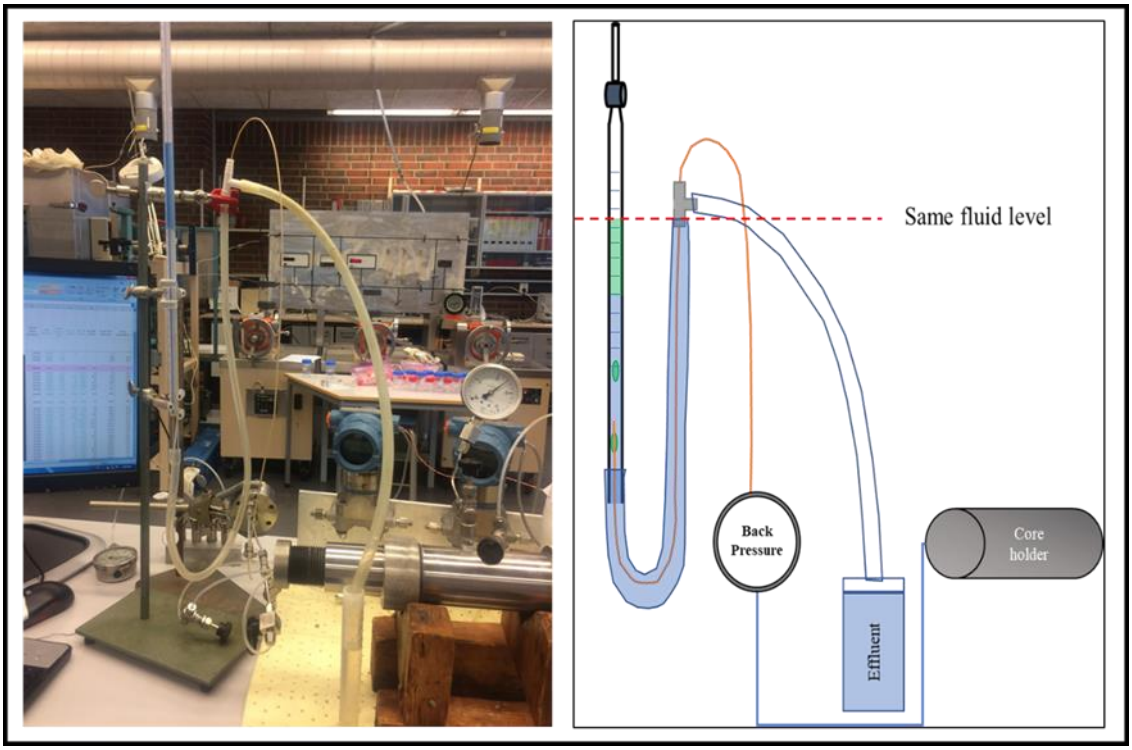

Figure 8. (Left) Pictures of the separator; (Right) Schematic of the separator.

4.3 Experimental Procedure

Figure 9 demonstrates general experiment steps that are conducted to the core. There are two types of treatment applied to the core depends on the wettability of the core. For mixed-wet core, saturation establishment is performed before wettability alteration. In the forced imbibition process, several values of rates are applied to retrieve the recovery performance and to estimate the negative value of capillary pressure to obtain residual saturation.

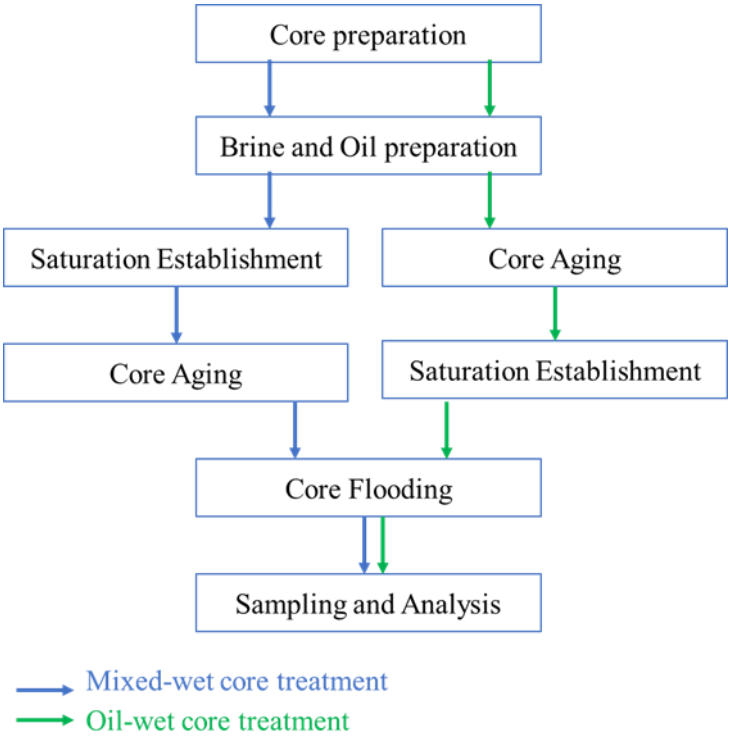

Figure 9. Schematic of experiment steps.

4.3.1 Core Preparation

In this stage, the dimensions of the core are measured by using a calliper to calculate the bulk volume of the core. The bulk volume of the core is calculated by using the formulation to measure cylinder (equation (29)) where D is the diameter of the core and L is the length of the core.

$$V_{bulk} = \frac{\pi}{4} \times \frac{D^2}{L} \tag{29}$$

Figure 10. Illustration of measuring the dimensions of the core.

4.3.2 Brine and oil preparation

4.3.2.1 Brine preparation

In this experiment, there are two solutions of sodium chloride with different concentration (1 M and 0.1 M). Firstly, 58.44 gram of NaCl (manufactured by VWR BDH Chemicals) is dissolved in distilled water to make one litre of Sodium Chloride 1 M. Then the brine is stirred overnight to form a homogeneous solution. Figure 11 illustrates the filtration setup. Stirred brine is filtered by using 0.22 µm filter paper and a filter to remove unwanted particle. Finally, brine is stored inside the plastic jar to prevent reaction with silica.

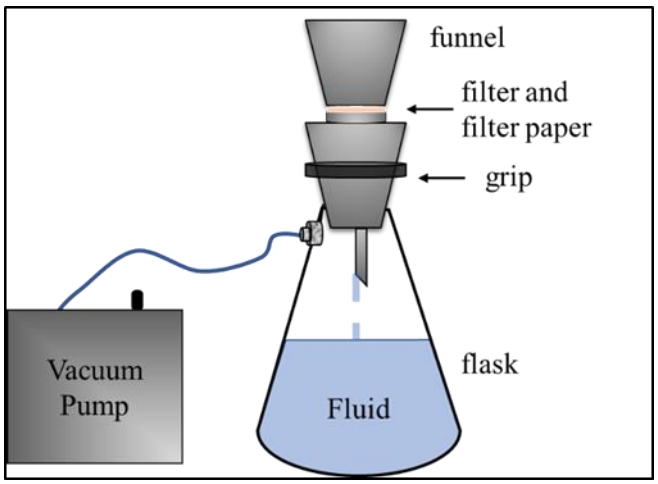

Figure 11. Filtration setup.

NaCl 0.1 M is made by adding distilled water to NaCl 1 M with proportion 90% distilled water and 10% NaCl 1 M.

4.3.2.2 Oil preparation and colouration

N-decane is used to saturate the core after initial water saturation establishment and to make Quilon in n-decane solution for changing the wettability. N-decane can be used without filtration process. The amount that of n-decane to saturate the core is 5 PV.

For the Bentheimer_3 experiment, Sudan Blue GN is added to n-decane. First, a tip of Sudan Blue GN is mixed to 20 mL of n-decane inside a small glass jar (Figure 12 (a)). It should be mixed instantly, but it is allowed to shake or even stir the jar with a magnet if needed. The syringe is used to collect and to add droplets to the main n-decane until the significant colour is seen (Figure 12 (b)). For additional, a tip of Sudan Blue GN can be added to distilled water to check the solubility with water. From Figure 12, it is proved that Sudan Blue GN is not soluble in distilled water.

Figure 12. Illustration of n-decane colouration. (a) a mixture between a tip of Sudan Blue GN and n-decane in a small glass jar; (b) a final mixture between a tip of Sudan Blue GN and n-decane that is injected to Bentheimer_3; (c) a mixture between a tip of Sudan Blue GN and DI Water in a small glass jar.

4.3.3 Initial Saturation Establishment

4.3.3.1 Saturating core with NaCl 1 M

Figure 13 represents a schematic of equipment used for core saturation. The core is placed inside the plastic container, and it is put inside a sealed setup. A vacuum pump is run to remove any air from the installation. The pressure in the setup should be lower than 0.6 mbar. Later, the vacuum pump is turned off, and the brine flows through a valve until the water column is higher than core height. When the core is fully saturated, it is taken out from the sealed setup, and the saturated core is weighed.

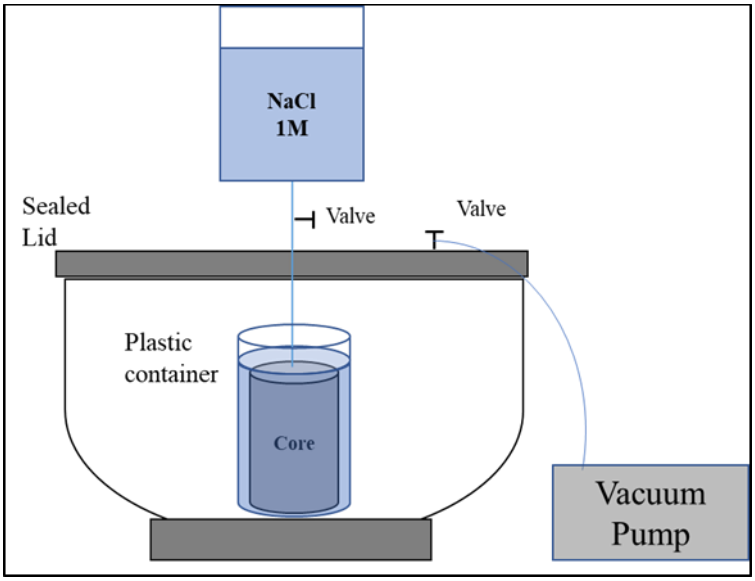

Figure 13. Schematic of equipment used for core saturation.

4.3.3.2 Porosity measurement

Porosity calculation is based on the weight difference between dry core and fully saturated core. The density of the brine is measured by a densitometer. The weight of the core is measured

by a scale that is manufactured by Mettler Toledo (see Figure 14). The pore volume of the core is calculated by equation (30). Moreover, porosity is computed using equation 31.

$$PV = \frac{m_s - m_d}{\rho_w} \tag{30}$$

$$\phi = \frac{PV}{V_{bulk}} \tag{31}$$

Where PV is the pore volume of the core (cm^3), m_s is the weight of saturated core (g), m_d is the weight of dry core (g), ρ_w is the density of brine (g/cm^3), ϕ is the porosity of core (fraction), and V_{bulk} is the bulk volume of the core (cm^3).

Figure 14. Illustration of weight measurement of the dry core of Bentheimer_1.

4.3.3.3 Absolute permeability measurement

Figure 15 illustrates the permeability measurement setup. The core is put inside the core holder, and brine flowed through the core. 26 bars of confining pressure and 6.5 bars of back pressure are applied in the setup. Two pressure gauges are used to measure the differential pressure between the inlet and the outlet of the core holder. One of the pressure gauges is used to measure the small range of the differential pressure up to 62 mbar. The other is used to measure a higher range up to 2.5 bar.

The flooding rates are 0.1, 0.25, 0.5, 1, 3 and 5 mL/min and then it reduces again to the lower value. The rates are kept until three pore volumes are reached. The effluent is collected at each step, and the differential pressure at a specific rate is measured. Since only brine flow through the core, then absolute permeability is measured. By using Darcy's law in the equation (3), the absolute permeability of core is calculated.

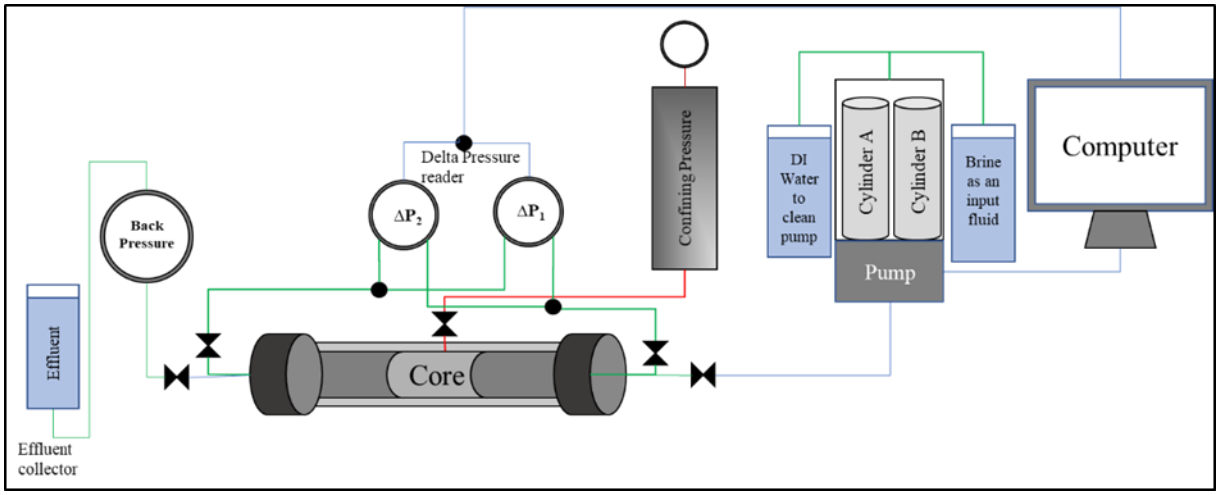

Figure 15. Permeability measurement setup.

The result of the permeability test is shown in chapter 5.2.

4.3.3.4 Initial water saturation set up

In this stage, desiccation principal is used to getting the desired initial water saturation. Figure 16 shows the desiccator equipment. The core is fully saturated with NaCl 0.1 M by injecting three pore volume of the core using core flood setup. By using NaCl 0.1 M, it is assumed that after desiccation procedure from 100% saturation to 10% saturation, it increases the salinity of NaCl 0.1 M to the same value as NaCl 1 M.

The saturated core is placed horizontally inside the desiccator. There are silica grains inside desiccator to improve evaporation process. These silica grains are changed regularly when the colour change from blue to orange. This desiccation process takes several days to reach the target initial water saturation. Therefore the weight of the core is frequently measured until it reaches the target. In this experiment, the target initial water saturation is 10% with the assumption that this value is below irreducible water saturation. The saturation is set to be small enough so that it is easier to identify when oil is produced in recovery profile evaluation. By using equation 32, the weight of the target is calculated.

$$m_t = (m_s - m_d)S_{wi} + m_d \quad (32)$$

Where m_t is the target weight of the core (g), m_s is the weight of saturated core (g), m_d is the weight of dry core (g), and S_{wi} is the initial water saturation (fraction).

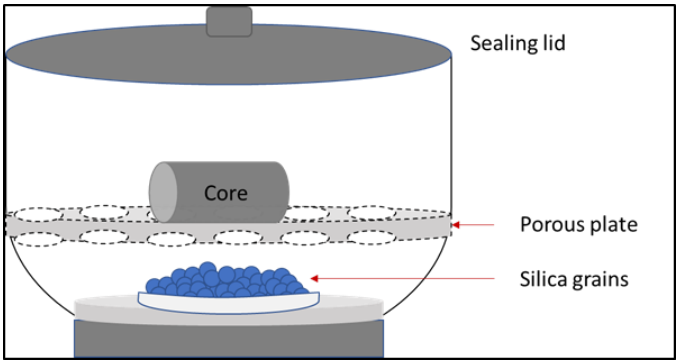

Figure 16. Desiccator setup.

When the weight of target is obtained, the core is taken out from desiccator equipment; then it is placed inside a container for a few days until it reaches equilibrium. During the desaturation process, the brine mostly is evaporated from the surface which means inside core is wetter than outside core. By leaving the core for a while, the brine in the centre part is expected to come out and create a uniform wet distribution in the core.

4.3.3.5 Initial oil saturation setup

In oil saturation setup, piston cell is added to core flood. The piston cell is used to prevent damage to the pump where oil is put in the upper part of the piston, and distilled water in the bottom part is used to push the piston to flow oil. Figure 17 illustrates a setup schematic of oil saturation, where oil is illustrated by the green colour inside the piston cell. The core with initial water saturation is placed inside oil saturation setup. Confining pressure of 26 bar and the back pressure of 6.5 bar is applied to the core holder. The experiment is done at the room temperature. Five pore volume of oil is injected with the rate of 0.5 mL/min in one direction. The variation in rates is applied to measure the oil effective permeability at initial water saturation.

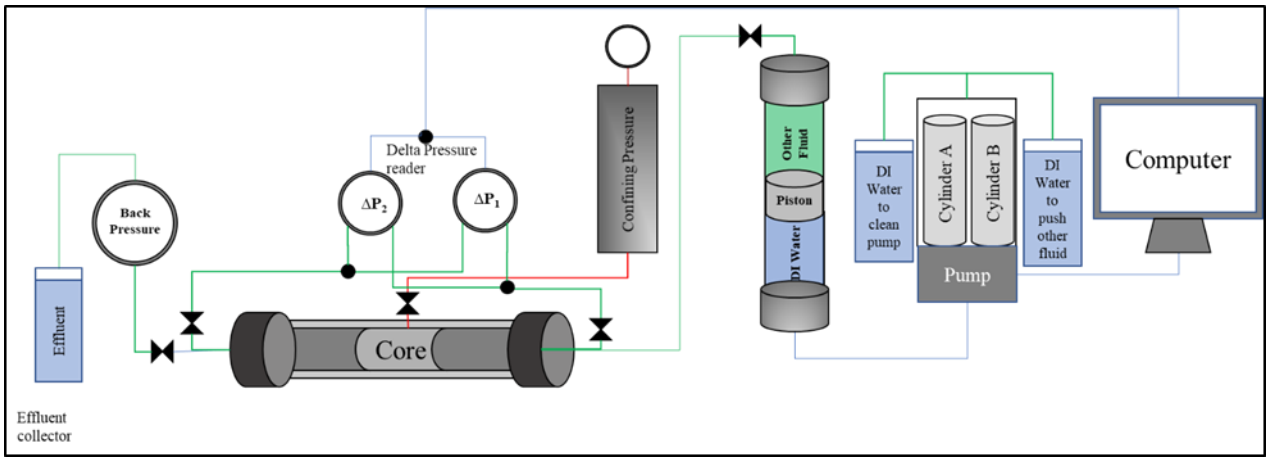

Figure 17. Initial oil saturation and Quilon solution injection set up.

4.3.4 Core Aging

4.3.4.1 Wettability Alteration

Different wettability alteration methods are applied to the core. In this thesis, the wettability of four cores is changed from water-wet to more oil-wet sandstones.

a. Mixed-wet

This step is executed after establishing initial saturation of water and n-decane. A solution of Quilon-L and n-decane is used to change the wettability of the Bentheimer core from strongly water wet to mixed wet. The modification of the core's wettability is based on a method which applied by Abeysinghe et al. (2012). During solution preparation, the contact with light is minimised by covering the equipment with aluminium foil to keep the stability of Quilon-L. The solution is made by mixing 3% weight of Quilon-H and 97% weight of n-decane. The solution is stirred for 30-45 minutes, and 0.22 µm filter is used in filtration set up (Figure 11). Afterwards, in each direction, the solution of Quilon-L in n-decane is injected into the Bentheimer_2 horizontally by using the fluid saturation set up horizontally (Figure 17) at the flow rate of 0.5 mL/min. Based on Abeysinghe et al. (2012), the Quilon-L in n-decane solution should be injected five PV in each direction. However, in this experiment, the colouration is reached after 9.52 PV injection of solution at the first direction and 5.74 PV at the second direction. Next, 13.72 pore volumes of n-decane are injected to flush out the solution of Quilon-L and n-decane. The effluent of n-decane should be clear.

b. Oil-wet

This step is executed when the core is in a dry condition. A method which is applied by Askarinezhad (2018) is used to modify the wettability of the core. Considering the sensitivity of Quilon towards the light, then all of the equipment is covered with aluminium foil to minimise the contact with light. The solution is created by mixing 3% weight of Quilon-L in distilled water. For about 45 minutes, the solution is stirred by using a magnet, and afterwards, it is filtered through 0.45 µm filter on filtration set up (Figure 11). By using the fluid saturation set up, 5 PV of the solution is pumped vertically (Figure 18) at the flow rate of 0.5 mL/min each in both directions. After finished Quilon solution injection, the core is taken out from the core holder and transferred to a dark oven with temperature 95^{o}C for one week. Finally, the core is stored at room conditions in a dark place before using it for other procedure.

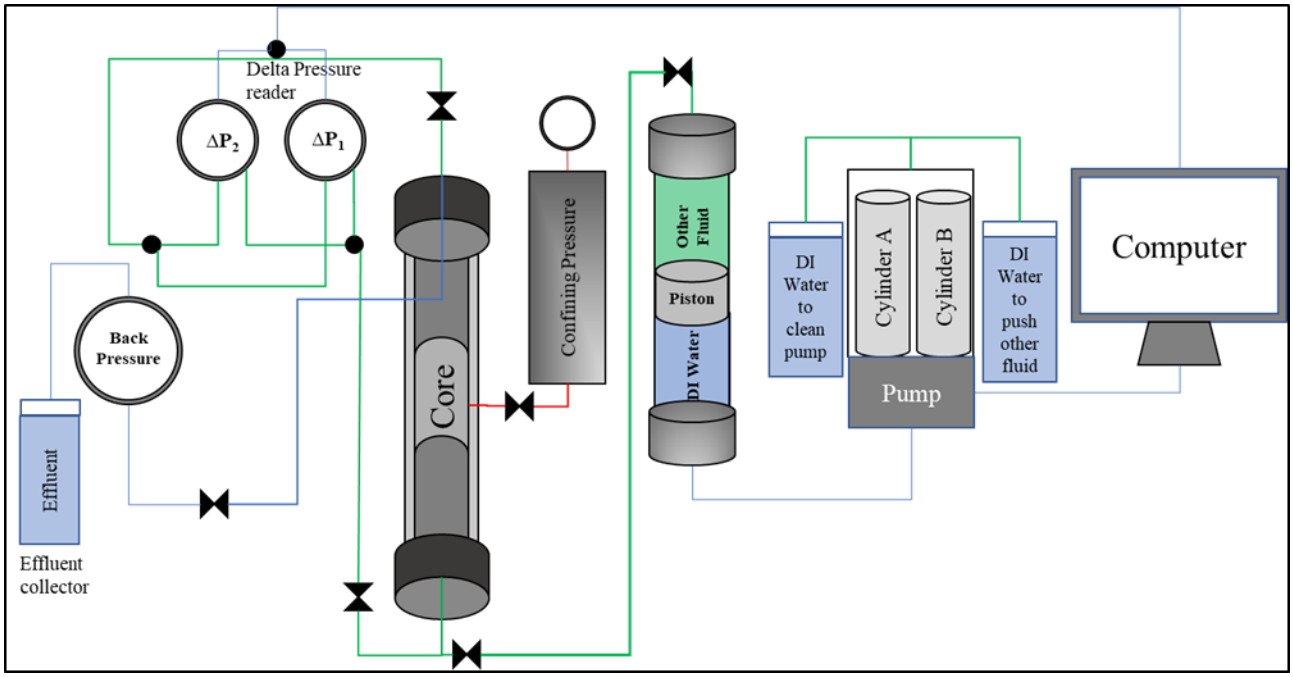

Figure 18. Illustration of wettability alteration equipment (vertical core holder.

4.3.5 Spontaneous Imbibition

Spontaneous imbibition is being tested by using Amott cell (Figure 19) that is manufactured by JM Glassteknikk Skandinavia AS Oslo at room temperature. There are two parts of the setup, bottom and upper parts. Firstly, marbles are put on the bottom part of the Amott cell. The purpose of doing this is to give spaces on the bottom of the core so that it is not covered and oil can also be produced from the bottom part. Then core is put inside the bottom part of the Amott cell and closed with the upper part. Grease should be applied to the wall of connection between two parts of spontaneous imbibition. Next, brine is flowed to Amott cell until certain level to facilitate the oil production measurement. Cumulative oil production of the core is measured from time to time, and it is plotted on the graph.

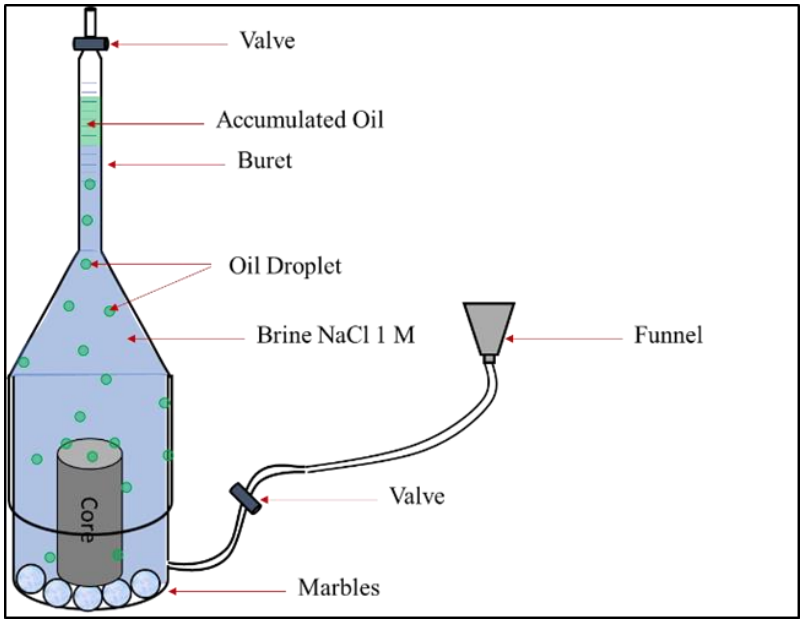

Figure 19. Spontaneous imbibition setup.

4.3.6 Core Flooding (Force Imbibition)

Core flooding is the central part of this experiment when brine is injected to the core after spontaneous imbibition. This process is called forced imbibition. The additional part in the setup compared to Figure 15 is the bypass line and the separator (Figure 20). By using a bypass line, a higher rate can be applied to increase the pressure in the system without damaging the core. By using the separator, oil production can be measured inside burette, and the brine is collected on the other effluent collector.

First, all the lines should be filled up with brine by using dummy core. Next, the dummy core is replaced by the real core. The vacuum pump is used to take out and to insert the core. Any air inside the system should be removed. Finally, the core flooding can be done.

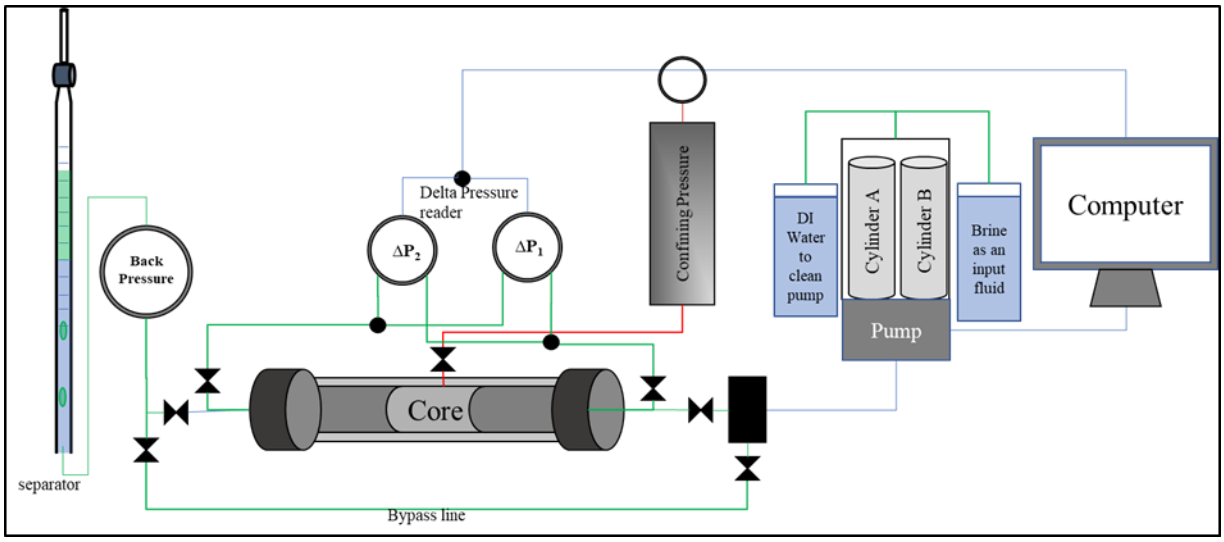

Figure 20. Core Flooding Setup.

During the experiment, several rates are applied to the core by increasing step by step (Chapter 5.6). The last rate is the maximum rate of the pump which is 7.5 mL/min. The rate can be changed if there is no additional oil production, steady pressure, and the rate of produced brine is equal to the rate of injected brine. This condition is consistent with the steady-state assumption in Chapter 2.4.

After applying all the rates, the same permeability test as in Chapter 4.3.3.3 is conducted to measure the effective permeability of water at the final water saturation from forced imbibition process.

5 Results and Discussion

5.1 Porosity measurement

By measuring the dimension of the core, bulk volume of the core can be calculated. The dry weight of the core was measured. Next, after saturating the core with NaCl brine, the weight of the saturated core was measured, and by using equation (30) and (31), and finally, the porosity of the core was calculated. Table 3 shows the porosity value for all the cores.

Table 3. Porosity and mass measurement for all the cores.

Parameter	Berea	Bentheimer_1	Bentheimer_2	Bentheimer_3
The bulk volume of the core (cm^3), V_{bulk}	99.72	100.82	101.09	100.71
The weight of dry core (g), m_d	202.91	203.36	205.30	205.24
The weight of saturated core (g), m_s	224.55	227.32	228.17	227.26
The pore volume of the core (cm^3), PV	20.84	23.07	22.02	21.98
Porosity %, Φ	20.89	22.89	21.79	21.82

5.2 Permeability measurement

Table 4 shows the permeability value for all the cores. There were four measurements of permeability that was conducted on this experiment. They were the absolute permeability, the effective permeability of oil at initial water saturation before and after wettability alteration, and the effective permeability of water at water saturation after forced imbibition.

Wettability Alteration of Bentheimer_1 was not successfully conducted(see chapter 5.4.1.2). Therefore, only the absolute permeability and the relative permeability of oil before wettability alteration were measured on Bentheimer_1. As for the Berea core, the effective permeability of water was measured even though the current saturation by volume was unknown. The core lost the confining pressure in the middle of the experiment, and the lost oil could not be tracked. The current saturation of Berea was measured by using the weight of the core. Berea and Bentheimer_3 did not have the value of effective permeability of oil before wettability alteration, since the wettability alteration procedure as conducted when the core was dry and clean.

Table 4. Permeability measurements for all the cores.

Parameter	Berea	Bentheimer_1	Bentheimer_2	Bentheimer_3
K, absolute permeability, Darcy	0.63	3.20	3.00	3.10
Before wettability alteration				
k_{oeff} at S_{wi} ,Darcy	-	3.12	3.00	-
k_{ro} at S_{wi}	-	0.98	1.00	-
After wettability alteration				
k_{oeff} at S_{wi} , Darcy	0.4	-	1.4	2.3
k_{ro} at S_{wi}	0.64	-	0.46	0.73
k_{weff} at S_w after forced imbibition, Darcy	0.45	-	0.08	1.54
k_{rw} at S_w after forced imbibition	0.72	-	0.08	0.5

The saturation measurement is explained in chapter 5.3.

5.2.1 Absolute Permeability

In all tests, the differential pressure over rate was measured by computer, except for Bentheimer_3 where it was measured manually. Figure 21 shows the rate and differential pressure of each core. According to Darcy's equation, the rate is proportional to differential pressure as it can be seen in Figure 21.

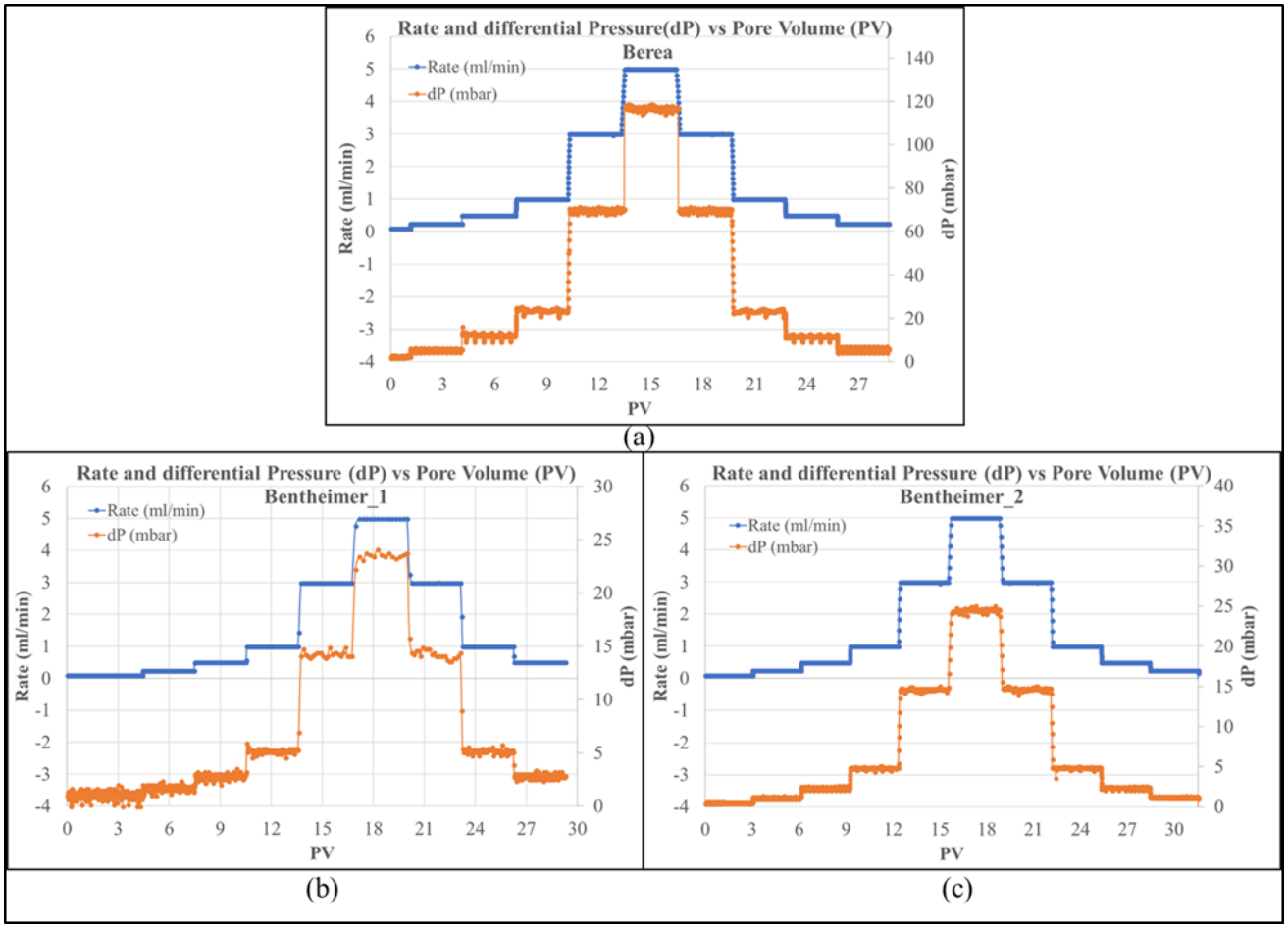

Figure 21. Permeability test for (a) Berea core; (b) Bentheimer_1; (c) Bentheimer_2.

5.2.2 Relative permeability of oil at S_{wi}

After initial water establishment, five pore volumes of n-decane was injected through the cores. By applying the different rate of n-decane to the core, the effective permeability of oil was calculated. Darcy's law (equation (3)) was used with the assumption that the initial water saturation was small enough, and no water was produced while injecting n-decane. The correlation between rate and differential pressure should be a straight line as can be seen in Figure 22. A higher rate was resulting in higher differential pressure. The value of effective permeability of oil at initial water saturation can be seen in Table 4. Relative permeability can be calculated as the ratio between the effective permeability of oil to the absolute permeability (equation (4)).

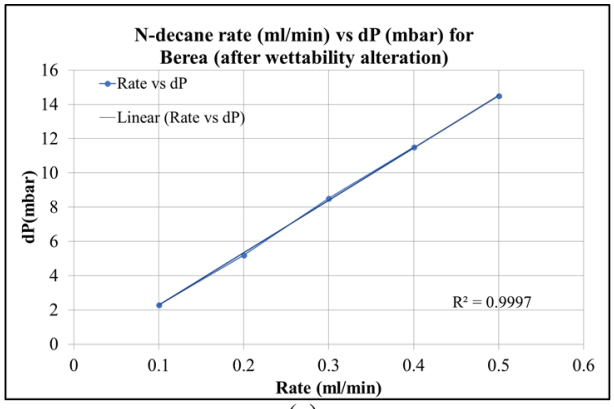

(a)

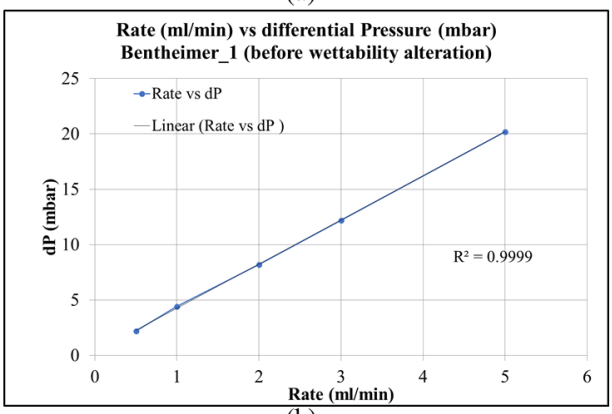

(b)

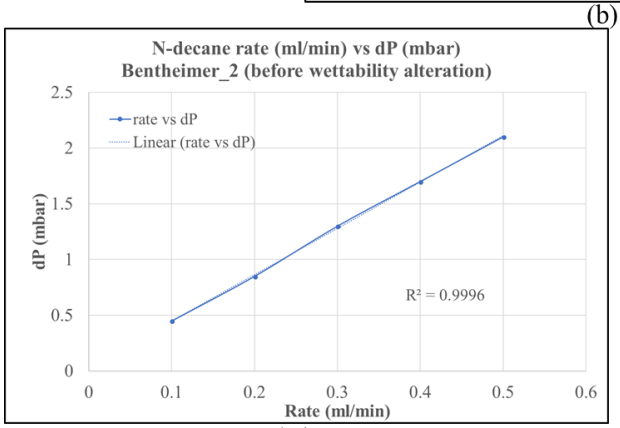

(c_1)

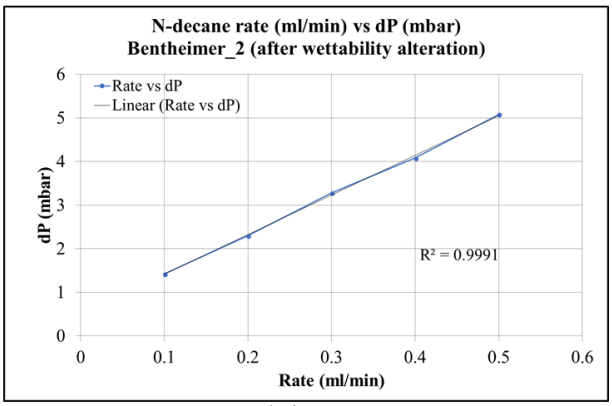

(c_2)

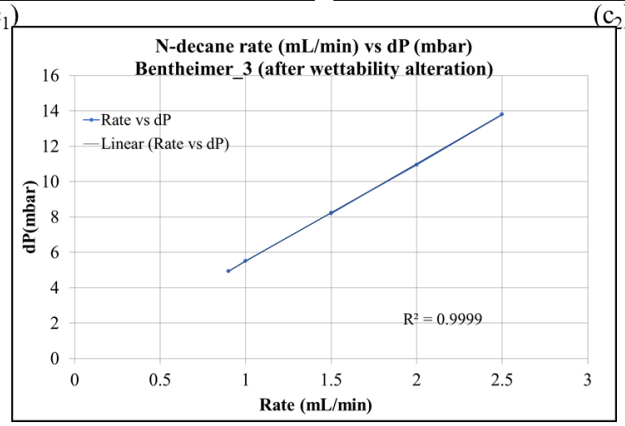

(d)

Figure 22. Correlation between n-decane rate vs differential pressure for (a) Berea; (b) Bentheimer_1; (c) Bentheimer_2; (d) Bentheimer_3.

The wettability alteration on Bentheimer_1 was not successfully conducted. Therefore, there was no value of effective permeability of oil after wettability alteration. The value of relative permeability of oil at initial water saturation for Bentheimer_1 and Bentheimer_2 were quite similar. It can be assumed that the wettability alteration on Bentheimer_2 was successfully performed because there was a change in relative permeability of Bentheimer_2 from 1 to 0.46.

As for Berea and Bentheimer_3, there was no measurement of effective permeability of oil because the wettability alteration for both cores was conducted when the core condition was dry.

5.2.3 Relative permeability of water at S_w after Forced Imbibition

After force imbibition procedure, brine was injected through the core in the different range of rate. It was assumed that there was no oil produced in this stage. By using Darcy's formulation (equation (3)), effective permeability of water after forced imbibition procedure was measured. Relative permeability of water was calculated as the ratio between the effective permeability of water an absolute permeability (equation (4)).

5.3 Saturation measurement

Table 5 shows the water saturation for each core. Three steps of water saturation were measured in the experiment. They were the initial water saturation, the water saturation after spontaneous imbibition procedure (Pc=0) and the water saturation after forced imbibition.

It was assumed that the initial water saturation was small enough for water to be immobile, and there was no additional water produced while injecting n-decane to the core. The core was desiccated by evaporation as mentioned in subchapter 4.3.3.4. The water saturation after spontaneous imbibition was obtained after letting water imbibe the core and replaced the oil until steady recovery was reached. Lastly, the water saturation was obtained after the forced imbibition procedure.

Table 5. Initial water saturation for each core.

Parameter	Berea	Bentheimer_1	Bentheimer_2	Bentheimer_3
Initial water saturation (%),S_{wi}	10.5	10.5	7.4	10.6
S_w after spontaneous imbibition (%)	11.8	-	41.5	10.7
S_w after forced imbibition (%) by using volume	-	-	53.2	80.3
S_w after forced imbibition (%) by using weight	73.2	-	58.8	81.9

The water saturation after forced imbibition was also calculated by using mass balance between total weight and dry weight (equation (33)) to cross check the value from cumulative oil calculation.

$$S_w = \frac{m_s - m_d - PV \cdot \rho_o}{PV \cdot (\rho_w - \rho_o)} \quad (33)$$

Where S_w is the saturation after forced imbibition, m_s is the weight of saturated core (g), m_d is the weight of dry core (g), PV is the pore volume of the core (cm^3), m_d is the weight of dry core (g), ρ_w is the density of brine (g/cm^3), and ρ_o is the density of oil (g/cm^3). After forced imbibition procedure, some oil can still be trapped by end effects so remaining oil saturation may not be equal to the true residual oil saturation.

5.4 Wettability alteration

Both Bentheimer and Berea are strongly-water-wet due to the quartz contents, while most of the reservoirs are not. Therefore, wettability alteration was performed to make it suitable for experimental study in which wettability plays a significant role.

5.4.1 Strongly water-wet to mixed-wet

Two cores were treated to change the wettability from strongly water-wet to mixed-wet. The wettability of Bentheimer_1 was not successfully conducted because Quilon-H was not soluble in n-decane. As for Bentheimer_2, the wettability was successfully conducted after changing Quilon-H to Quilon-L.

5.4.1.1 Stability of Quilon-H in n-decane

Based on Abeysinghe et al. (2012), Quilon-L should be used to perform wettability alteration. However, Quilon-H was used at the beginning of the experiment due to the availability with the assumption that it would behave the same as Quilon-L since the fluid properties of both chemicals are quite the same (See Table 2). However, as can be seen in Figure 23 the Quilon-H was not soluble in n-decane since there is residue or particles attach to the glass. Quilon-H was even separated from n-decane when it was taken out from piston cell after several days.

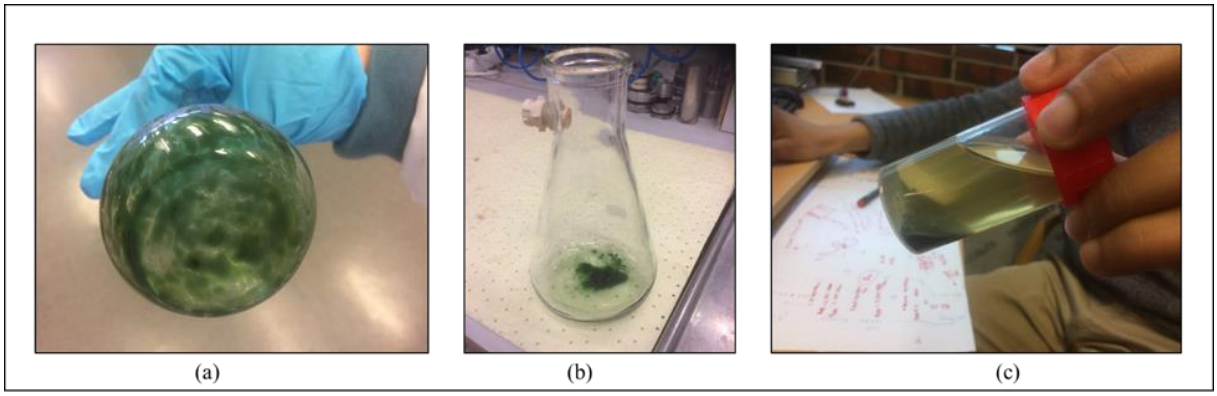

Figure 23. Solution residue of Quilon-H in n-decane: (a) after stirring the solution; (b) after filtering solution; (c) after taking out from the piston cell.

5.4.1.2 Injection of Quilon- H in n-decane to the core

There is no study about the solubility of Quilon-H in n-decane. At that time, the wettability alteration was still conducted without knowing that Quilon-H was not soluble in n-decane and only Quilon-H was available at that time. The procedure was adapted from Abeysinghe et al. (2012). After saturating the core with 10.51 % of NaCl 1 M and 89.49% of n-decane, five pore volumes of the solution of Quilon-H in n-decane was injected into each direction of the core, and five pore volumes n-decane was injected on the second direction to flush out the solution.

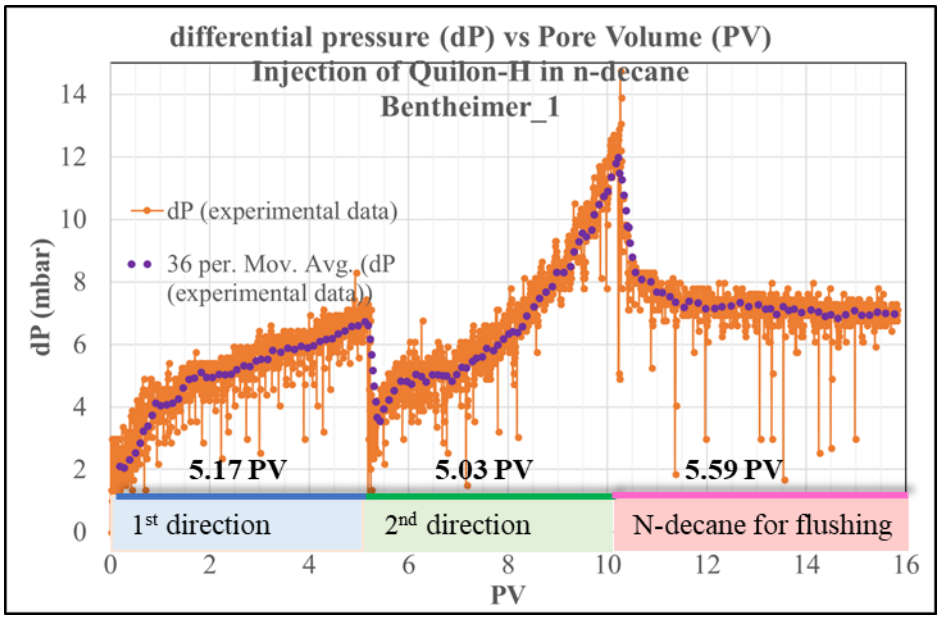

Figure 24. Differential pressure behaviour of injection of Quilon-H in n-decane on Bentheimer_1

Figure 24 shows the differential pressure behaviour of injection of Quilon-H solution. The differential pressure was increasing at the beginning due to differences in viscosity when the solution was flushing out n-decane inside the core and due to particles clogging the core. The trend of differential pressure on the second direction was sharper than in the first direction. It

is possible because the solution was also flushing out the residue of the solution in the first direction and probably particles or residue was clogging on the entrance of the first direction. Afterwards, n-decane was injected into the second the direction of the core. The differential pressure had a significant decrease at the beginning and then slightly decrease after injecting one pore volume of n-decane.

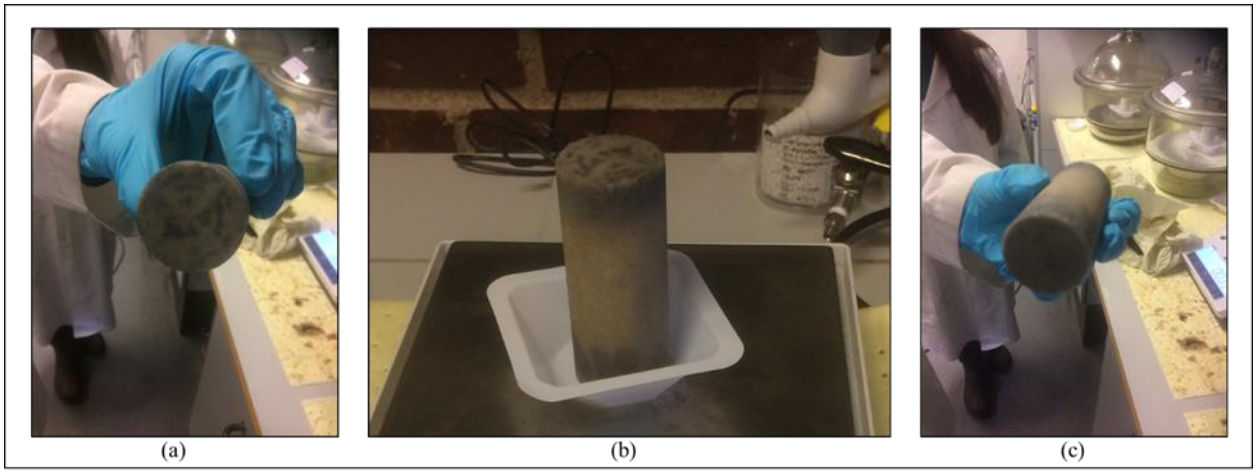

Figure 25. Condition of Bentheimer_1 after wettability alteration (a) inlet of the 1st direction; (b) whole core; (c) inlet of the 2nd direction.

Figure 25 shows the condition of the core after the wettability alteration. The solution was not reacted homogeneously inside the core. The core had a darker colour on the entrance of injection. It could be occurred due to the solubility of Quilon-H in n-decane and due to the residue or particles that got stuck from the previous injection. The effective permeability of oil was not measured. The wettability alteration was considered unsuccess since the colour of the core was not homogeneous.

5.4.1.3 Stability of Quilon-L in n-decane

In the end, Quilon-L is used in the experiment. With the same procedure from Abeysinghe et al. (2012), 3% weight of Quilon-L was mixed with 97% weight of n-decane. Quilon-L is more soluble in n-decane compared to Quilon-H. There was no particles or residue attached to the glass (See Figure 26).

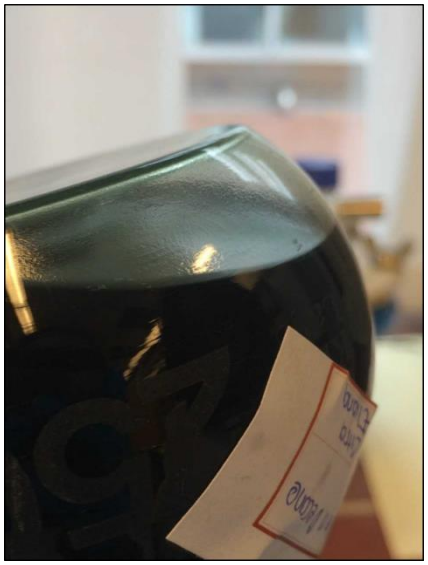

Figure 26. Solution of Quilon-L in n-decane.

5.4.1.4 Injection of Quilon- L in n-decane to the core

Based on the previous failure of wettability alteration on Bentheimer_1, there was a modification on the amount of injected volume. After saturating the core with 7.4 % of NaCl 1 M and 92.6 % of n-decane, Quilon-L in decane was injected. The injection was stopped when either colouration or the steady differential pressure was reached.

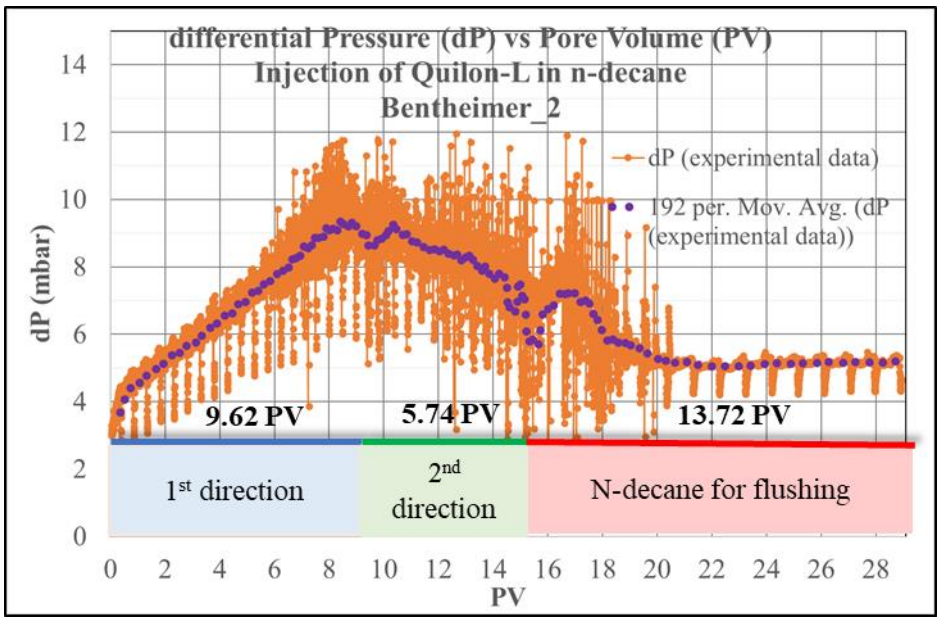

Figure 27. Differential pressure behaviour of injection of Quilon-L in n-decane on Bentheimer_2.

Figure 27 shows the differential pressure of injection Quilon-L in n-decane on Bentheimer_2. There was no viscosity measurement on the solution of Quilon-L in n-decane. However, from the physical appearance, Quilon-L was more viscous than n-decane. Therefore, it can be assumed that the viscosity of the solution Quilon-L in n-decane was higher than the viscosity

of n-decane. The differential pressure was increasing in the first injection due to the viscosity difference. When the solution was injected in the second direction, the pressure slightly increased in the beginning and then decreased. It happened because the effective permeability of oil inside the core had changed. As mentioned in chapter 4.3.4.1, the fatty-acid group in the Quilon is hydrophobic (Quilon data sheet, 2018). Therefore, the rock surface became hydrophobic because of the reaction between Quilon and the rock surface. The injection of Quilon solution was stopped when the colouration was reached.

N-decane was injected to flush out the solution from the core. The differential pressure decreased at the beginning of n-decane injection due to the lower viscosity. It slightly increased stabilised injecting around six pore volumes of n-decane.

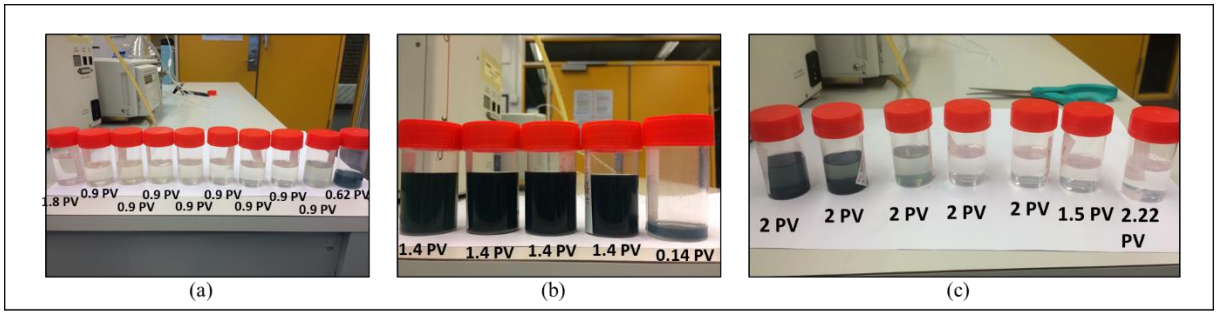

Figure 28. Effluent of injection Quilon-L in n-decane for Bentheimer_2: (a) the first direction of injection; (b) the second direction of injection; (c) n-decane flushing out.

Figure 28 shows the colouration of the effluent of the wettability alteration procedure on Bentheimer_3. In the first direction, the effluent colour was like the colour of n-decane. It got darker as the injection continued. The colour of the effluent was like the colour of the solution after 9.62 pore volumes of the solution was injected (Figure 28(a)). In the second direction, the colour of effluent was like the colour of the solution since the beginning of the second injection. The colour of effluent on n-decane injection changed from a darker colour to lighter colour.

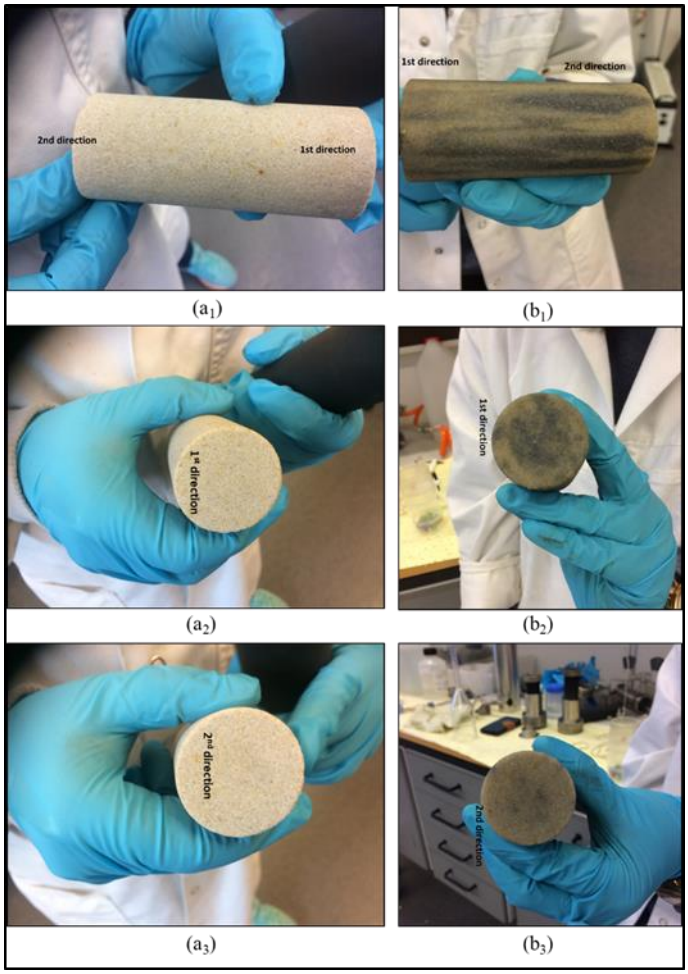

Figure 29. Condition of Bentheimer_2 after wettability alteration (a) whole core; (b) inlet of the 1st direction; (c) inlet of the 2nd direction.

The colouration after wettability alteration treatment was more homogenous for Bentheimer_2 (Figure 29) than Bentheimer_1(Figure 25). The wettability alteration on Bentheimer_2 was considered a success since the effective permeability changed from 3 Darcy to 1.4 Darcy.

5.4.2 Strongly water-wet to oil wet

Berea core was obtained pretreated. Therefore, there was no experimental data for differential pressure on Berea. By using the same procedure from Askarinezhad (2018), the wettability of Bentheimer_3 was changed.

5.4.2.1 Stability of Quilon-L in distilled water

The solution Quilon-L in distilled water was made by adding 3% weight of Quilon-L to 97% weight of distilled water. As can be seen from Figure 30, the solution was soluble in distilled water. There was no residue or particle attached in the glass that was used to stir the solution and inside the piston cell.

Figure 30. Quilon-L in distilled water: (a) after pouring the solution to filtration setup (b) solution left over inside piston cell.

5.4.2.2 Injection of Quilon-L in distilled water to the core

Since the experiment was performed vertically, there was gravity correction on the differential pressure. Figure 31 shows the differential pressure behaviour(after gravity correction) of Quilon-L in DI water injection on Bentheimer_3. Approximately, five pore volumes were injected in each direction of the core. In the first direction, the pressure increased from around 2.2 mbar, and it was stabilised at around 2.6 mbar. In the second direction, the pressure increased from around 2.5 mbar, and then it stabilised at around 2.6 mbar. The pressure increased sharply in the beginning because there was no fluid inside the core, and it stabilised when all of the pores were filled with the solution of Quilon-L in DI water. In the second direction, the core was already filled with the fluid. Therefore, the change of differential pressure on the second direction was smaller compared to the first direction. The differential pressure stabilised after injecting three pore volumes on the second direction.

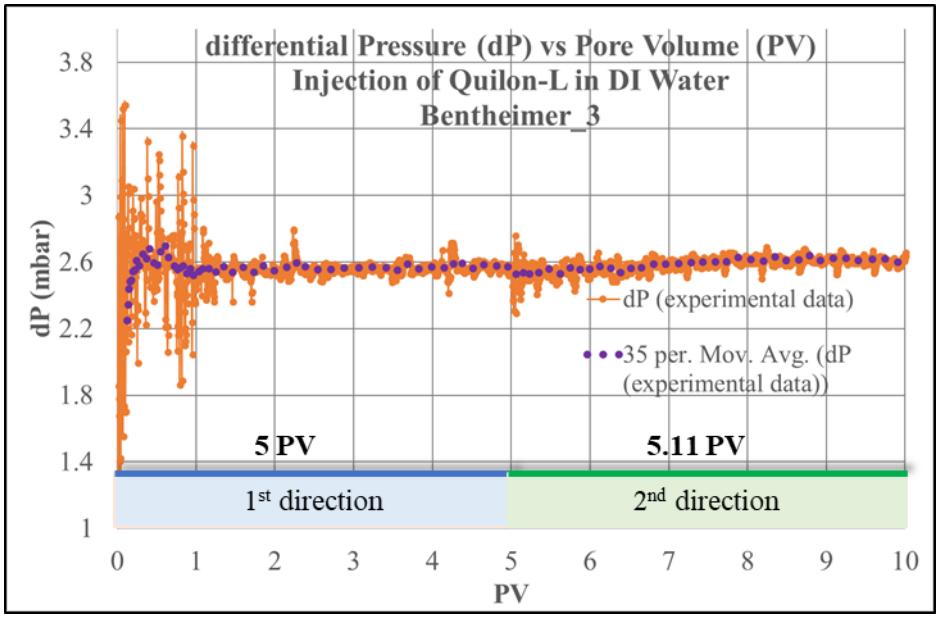

Figure 31. Differential pressure behaviour of injection of Quilon-L in DI water on Bentheimer_.3

Figure 32 shows the effluent of Quilon-L in distilled water for Bentheimer_2. Even though it cannot be seen clearly, the colour of effluent was lighter at the beginning of injection in the first direction. It was caused by the reaction between the solution and the core and resulting in the lighter colour of effluent.

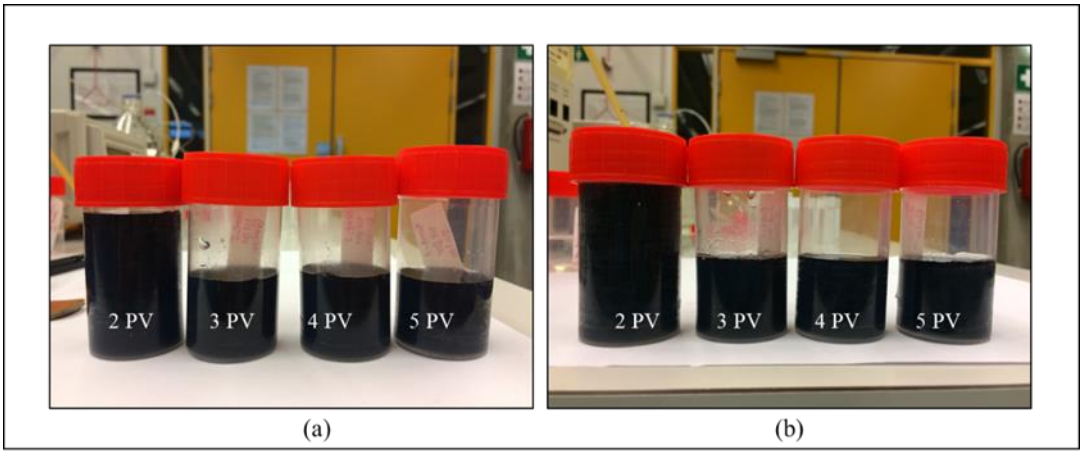

Figure 32 Effluent of Quilon-L in DI Water for Bentheimer_3: (a) the first direction of injection; (b) the second direction of injection.

After injecting Quilon-L in distilled water to the core, the core was placed inside the oven with a temperature of 95°C for a week. The core was placed hanging in the middle of the oven to dry it homogeneously. Figure 33 shows the physical properties of the core after Quilon-L in distilled water injection and after putting in the oven. The colour of the core was changing to green due to the colour of Quilon-L.

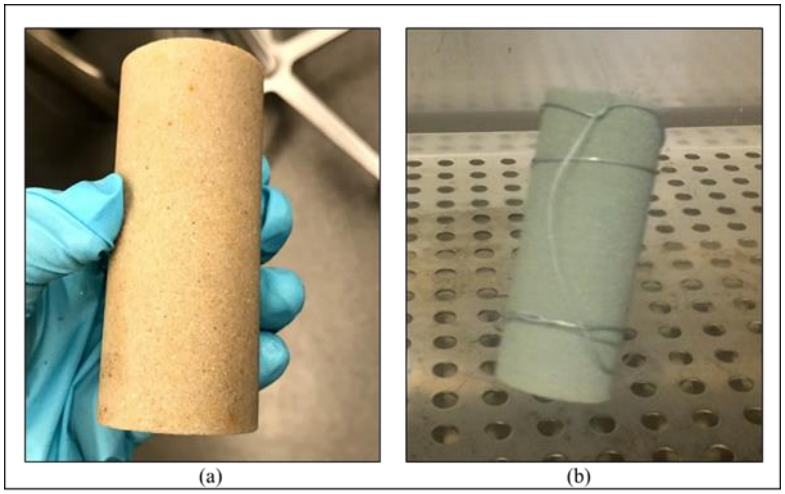

Figure 33. (a) Bentheimer_3 after injection; (b) Bentheimer_3 after putting in the oven.

The wettability alteration of Bentheimer_3 was successfully performed since the effective permeability of oil at initial water saturation was changing from 3 Darcy to 2.3 Darcy by using references from the effective permeability of oil at initial water saturation for Bentheimer_1 and Bentheimer_2 at the initial state (strongly water-wet). The recovery of oil from spontaneous imbibition was only 0.05 %. (See Figure 34)

5.5 Spontaneous Imbibition

Spontaneous imbibition was performed by using the imbibition cell. The cumulative oil over time was measured. Oil recovery from spontaneous imbibition was calculated by using equation (34) :

$$Oil\ Recovery\ (\%) = \frac{Cumulative\ oil\ produced\ (ml)}{Initial\ Oil\ in\ Place\ (ml)} \times 100\% \qquad (34)$$

Figure 34 shows the oil recovery after the spontaneous imbibition procedure for all of the cores. The oil recovery for Berea and Bentheimer_3 were minimal because they were oil wet, 1.2% and 0.05% respectively. The oil recovery for Bentheimer_2 was stable at 34.1 %.

Figure 34 shows the water saturation after spontaneous imbibition procedure for all of the cores. The initial water saturation of Berea was 10.5%, and it slightly increased to 11.8%. The initial water saturation of Bentheimer_2 was 7.4%, and it significantly increased to 41.5% after spontaneous imbibition. For Bentheimer_3, the water saturation increased from 10.62% to 10.67%. If the core is strongly water-wet, the oil will produce faster than a less water-wet core (Amott, 1959). Berea and Bentheimer_3 were more oil wet than Bentheimer_2 because of the value of the final oil recovery and water saturation after spontaneous imbibition is smaller than

Bentheimer_2 and also because they were prepared with a procedure that should make them oil-wet.

Wettability is an essential parameter on capillary end effect. It determines the interval between the saturation at the outlet (P_c=0) and residual oil saturation. The end effect is more significant when this interval is large enough (away from $(1 - S_{or})$ and closer to S_w when capillary pressure is equal to zero). In this experiment, capillary end effect on Bentheimer_3 is expected to be more significant than on Bentheimer_2.

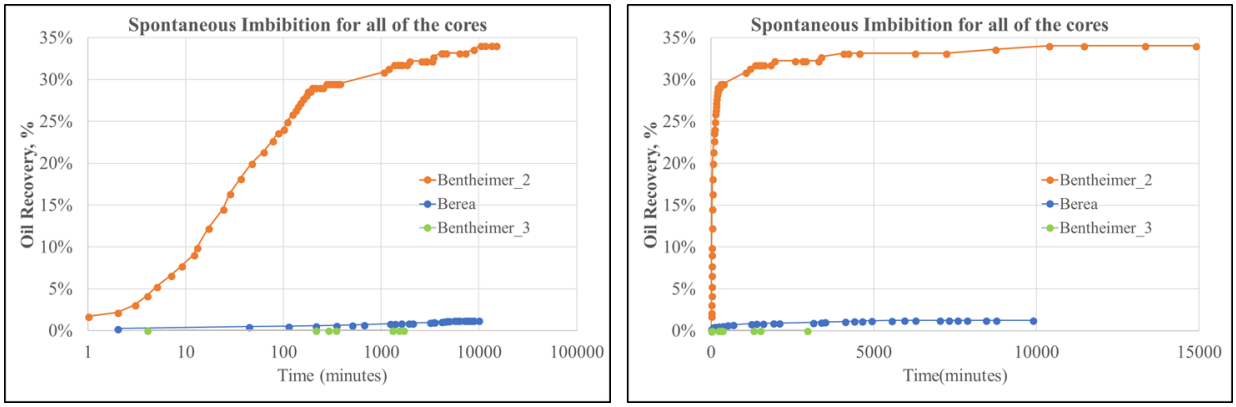

Figure 34 Oil recovery after spontaneous imbibition for all of the cores (Left: Log time; Right: linear time).

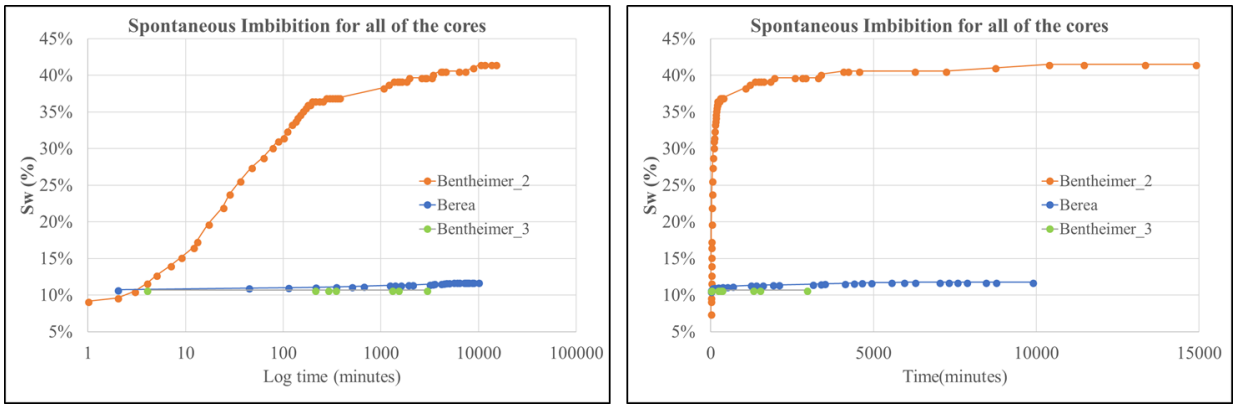

Figure 35. Water saturation after spontaneous imbibition for all of the cores (Left: Log time; Right: linear time).

5.6 Forced Imbibition

Forced imbibition was applied by varying the rates after the steady-state condition was reached. The flooding rates 0.4, 0.6, 1.2, 2.4, 4.8, 9.6, 19.2, 38.4, 76.8, 153.6, 307.2 pore volumes per day and the maximum rate of the pump (7.5 mL/min) were applied on the force imbibition on Berea, Bentheimer_2, and Bentheimer_3. Berea also applied 0.2 pore volumes per day in the beginning. However, due to the stability of the back pressure, it was decided to start the injection at 0.4 pore volumes per day on Bentheimer_2 and Bentheimer_3.

The system pressure (core and all the connections in the setup) should be larger than the back pressure for the fluid can flow out of the system. Back pressure was used mainly to have constant pressure above atmospheric pressure and to avoid forming of gas due to evaporation. Berea core has a lower absolute permeability compared to Bentheimer cores. Therefore, it took more time to reach the system pressure larger than the back pressure especially when the flow rate was really low (0.0029 mL/min). At that time, bypass line was not installed, and it took more than three days to increase the system pressure. In the end, it was decided to increase the system to 5.5 bar by increasing the rate. However, the negative side was the oil was being pushed out of the core by the high rate, not the low rate. By experiencing Berea experiment, it was decided to add bypass line to the core flood system on Bentheimer_2 and Bentheimer_3 to increase the system pressure without affecting the core.

While injecting the brine through the system, initially all of the lines were filled with brine. Therefore, the dead volume inside the outlet flow line was considered on the cumulative oil calculation. The corrected time or pore volumes can be calculated as

There was no dead volume correction on the measured differential pressure.

5.6.1 Berea

Figure 36 shows the experimental result of Berea. Total 185.7 pore volumes of brine were injected to the core. The first stable production on Berea occurred after approximately 0.5 pore volumes of water injection, and water saturation values increased from 11.7% to 32.9% at the first rate (0.2 PV/day). Since a steady-state was reached, there was no oil production. Therefore, high initial rate made an impact. After injecting 3.04 pore volumes in total, the system lost the confining pressure at the second rate (0.4 PV/day). The oil was seen not only in the outlet flowline but also inside the pressure lines that was connected to the outlet flowlines. The oil came out from the core to the pressure line due to the differential pressure after losing the confining pressure, not because of the forced imbibition procedure. The core flooding was continued while expecting that the effect of losing confining pressure was not too significant. However, the incremental of oil was only measured right after the lost confining pressure and on the last rate. After losing the confining pressure the water saturation increased from 36% to 40%, and the final water saturation was 66.2% on the last rate. The value of water saturation by measuring the weight of the Berea core after forced imbibition was 73.2%. The lost oil was probably due to the difficulty of measurement after losing the confining pressure, oil was everywhere, even inside the core holder.

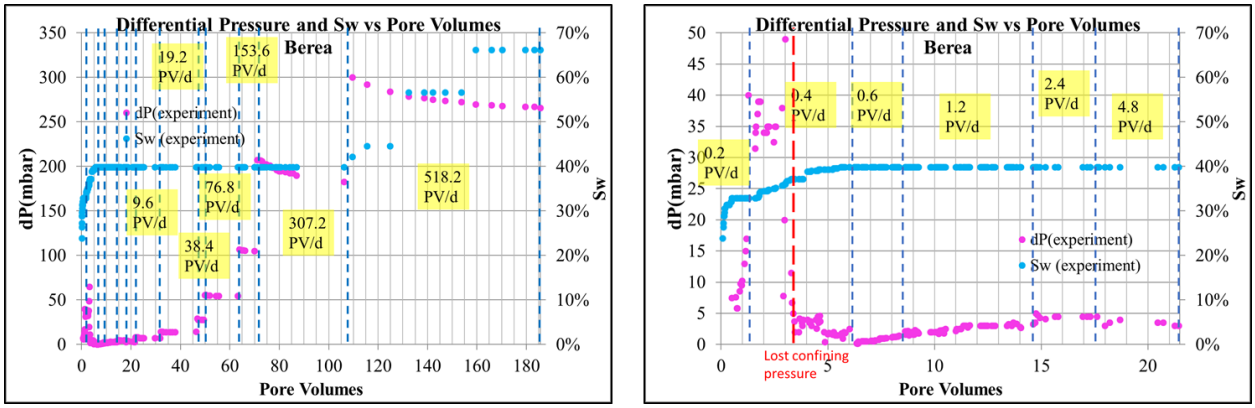

Figure 36) Differential Pressure and Sw vs Pore Volumes Berea: (Left) for all rates; (Right) for earlier rates.

5.6.2 Bentheimer_2

Figure 37 shows the experimental result from forced imbibition of Bentheimer_2. Total 302.4 pore volumes of brine were injected to the Bentheimer_2. The first stable production on Bentheimer_2 occurred after approximately 1.8 pore volumes of water injection, and water saturation values increased from 41.5% to 50.7% at the first rate (0.4 PV/day). The oil production mostly happened at the first rate. There was no oil production when the injected rates were 38.4 and 76.8 pore volumes per day. The increased water saturation from the second rate to the final rate was only 2.5%. Total cumulative oil during forced imbibition was 2.58 mL or equal to 11.7% water saturation. The final water saturation after forced imbibition was 53.2%. The value of water saturation by measuring the weight of the Bentheimer_2 core after forced imbibition was 58.8%. The difference in water saturation was not too significant. The lost oil probably occurred when the core demounted from the core holder and probably due to the flow line became more oil-wet because of the Quilon injection.

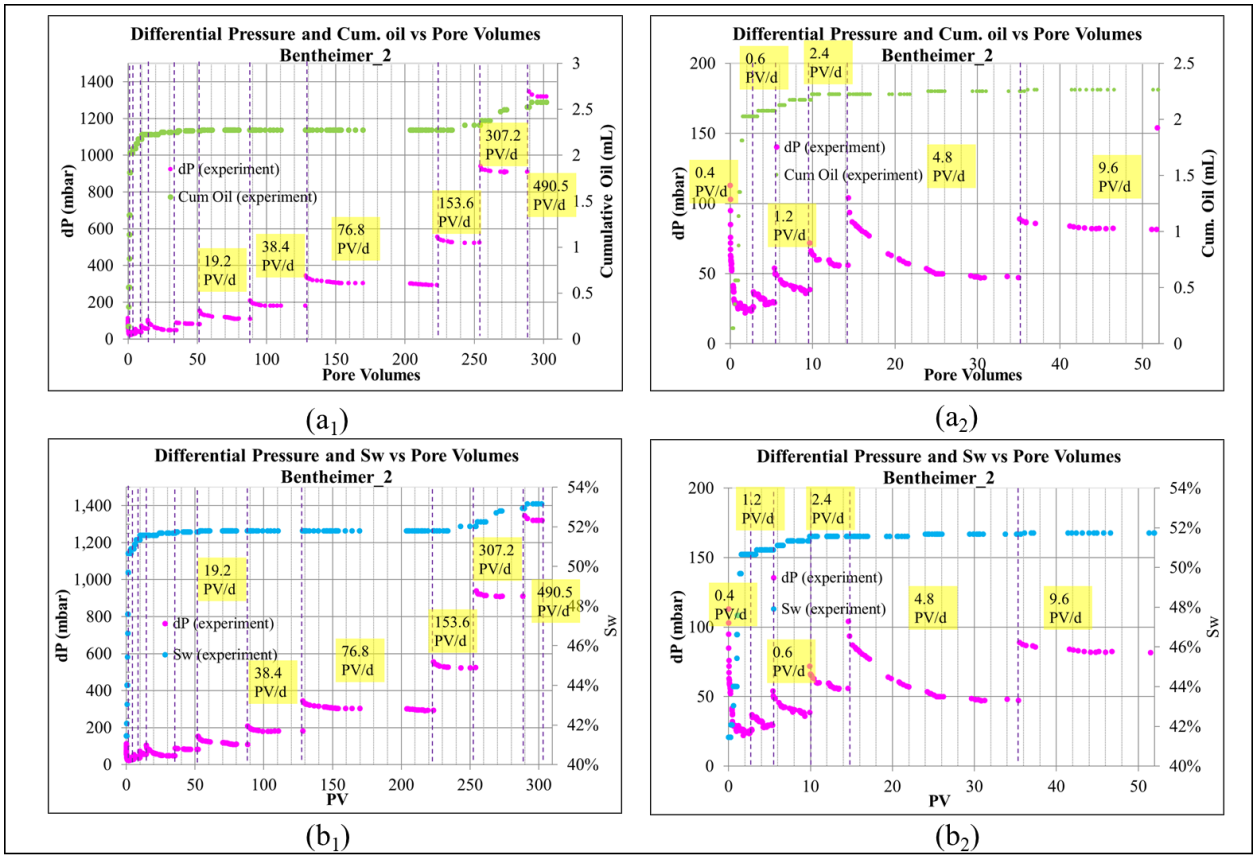

Figure 37. Forced Imbibition Result of Bentheimer_2 (a) Differential Pressure and cumulative oil vs Pore Volumes: (1) for all rates; (2) for earlier rates; (b) Differential Pressure and Sw vs Pore Volumes: (1) for all rates; (2) for earlier rates.

5.6.3 Bentheimer_3

Figure 38 shows the experimental result from forced imbibition of Bentheimer_3. The differential pressure on Bentheimer_3 was calculated by using basic fitting in Matlab for averaging since there were fluctuations in computer data. Total 149.1 pore volumes of brine were injected to the Bentheimer_3. Water breakthrough on Bentheimer_3 occurred after approximately 0.3 pore volumes of water injection, 2.2 mL oil produced, and water saturation values at 20.7%. The oil mostly produced on the first rate. Total cumulative oil during forced imbibition was 15.3 mL or equal to 69.6% water saturation. The production of oil mostly happened on forced imbibition (69.6%) compared to spontaneous imbibition (0.05%).

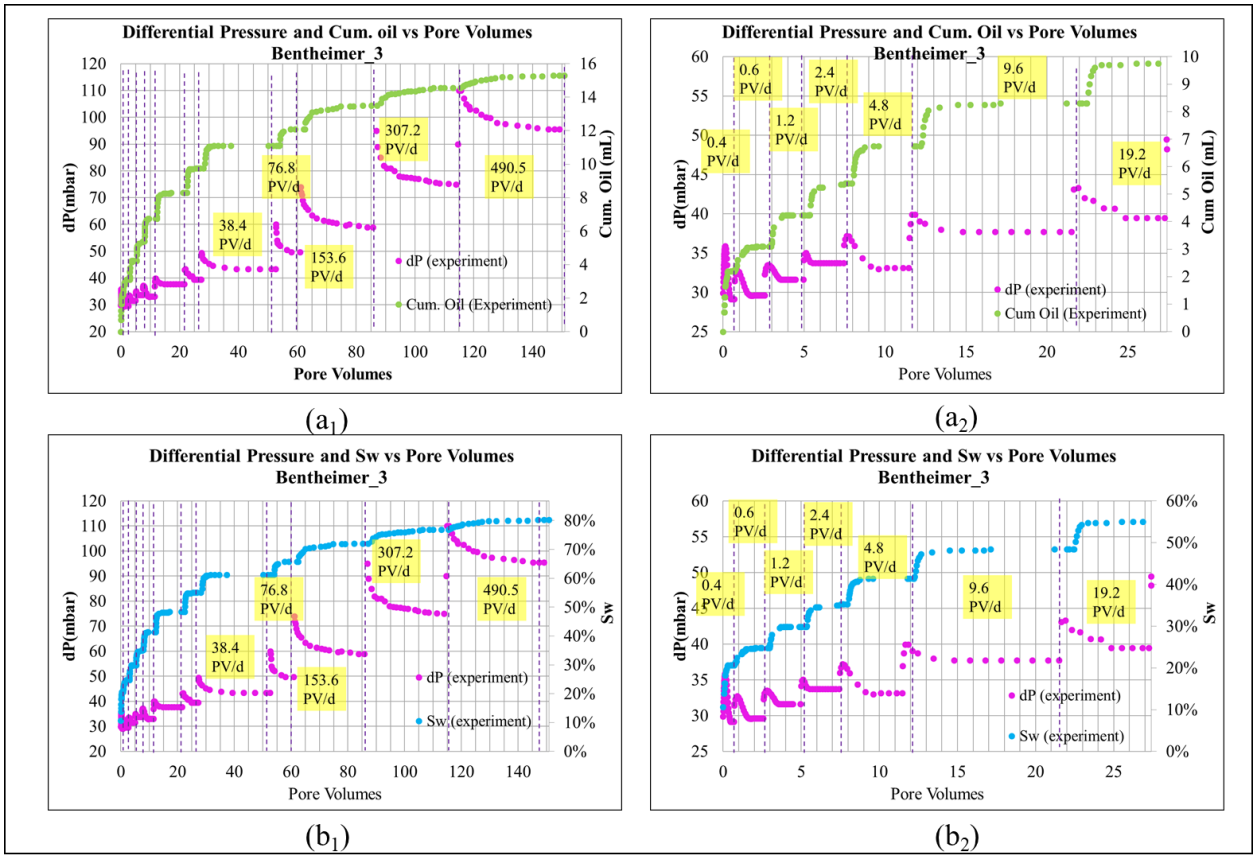

Figure 38. Forced Imbibition Result of Bentheimer_3 (a) Differential Pressure and cumulative oil vs Pore Volumes: ($_1$) for all rates; ($_2$) for earlier rates; (b) Differential Pressure and Sw vs Pore Volumes: ($_1$) for all rates; ($_2$) for earlier rates.

According to Gupta and Maloney (2016), the capillary end effect region has a flow rate dependence, and it decreases with the increase in the total flow rate. It was also shown that the wettability is affecting the capillary end effect. The capillary end effect is more significant on the core with more-oil wet compared to water-wet (Abeysinghe et al., 2012; Virnovsky et al., 1995). All the cores had capillary end effect since there was rate-dependency. However, the most significant capillary end effect was on Bentheimer_3 because it was more oil-wet compared to the other cores.

6 Numerical Analysis

6.1 History Matching by using SENDRA

The insufficient capillary end effect was observed on Bentheimer_2. End effects were demonstrated on a very narrow saturation interval. The functions could not be determined for most saturation. Therefore Bentheimer_3 was chosen for numerical analysis. Table 6 shows the input properties in SENDRA simulation, the left section shows the given values from experimental data, while the right section shows the determined values to create capillary pressure and relative permeability curves.

Table 6. Input properties in SENDRA and Corey and Skjæveland parameter for history matching.

Parameter		Corey parameter	
ϕ , porosity	0.2174	N_w	2.4
Base permeability [D]	3.1	N_o	2.5
Initial Saturation	0.1067	Krw (Sor)	0.7
Length [mm]	90.03	Kro (Swi)	0.73
Diameter [mm]	37.74	Skjæveland parameter	
Grid blocks in the x-direction	100	C_w	20
μ_o [cp]	1.09	A_w	0.6595
μ_w [cp]	0.92	C_o	2750
Saturation values		A_o	0.2684
Swi	0.1062		
Sor	0.132		

In the input properties of SENDRA, initial water saturation means the saturation at capillary pressure equal to zero after spontaneous imbibition (10.67%). While in the input analysis of SENDRA, initial water saturation means the real initial water saturation after desiccation procedure (10.62%). From Table 4 and Table 5, the final water residual oil after forced imbibition was 0.181 and average relative permeability of water at that saturation was 0.5. The effective permeability of water was measured after forced imbibition by measuring the differential pressure at different rates. Then, the average relative permeability of water can be calculated by using equation (4). In the simulation, it was assumed that Bentheimer_3 had a lower residual oil saturation 0.132 (i.e. if the higher rate were applied then more oil would be produced) and higher relative permeability of water 0.73. It was allowed to have a lower residual oil saturation since some oil could still be trapped by capillary end effects and that would also affect the relative permeability of water. According to Hadley and Handy (1956),

the change in residual water saturation is not very critical, and it will give a small percentage change in the end effect. Therefore, based on that study, lower residual oil saturation was used in the simulation.

Figure 39 shows the result of relative permeability curve matching Corey and capillary pressure from Skjæveland equation. The shape of the capillary pressure curve for oil-wet core corresponds to Masalmeh (2001) that the oil-wet capillary pressure curve drops to the negative value before continuing gradually towards more to a negative value. These curves were produced by matching the experimental data.

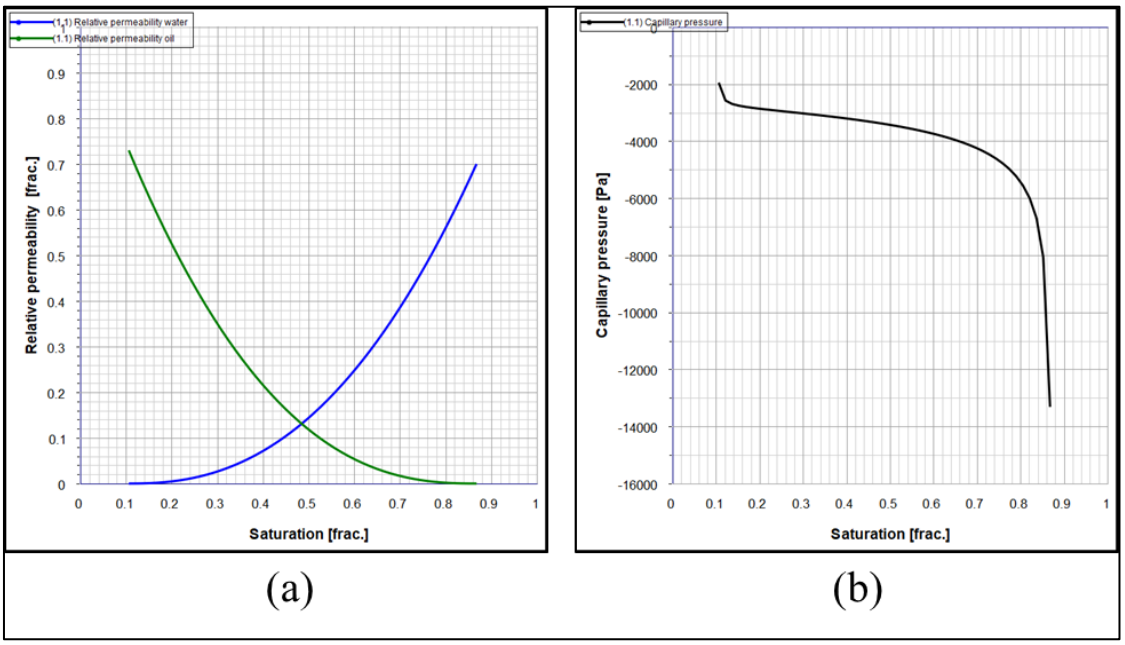

Figure 39. Relative permeability and capillary curves for Bentheimer_3.

Since the difference in the result of differential pressure and oil production that was obtained from these curves and the actual experimental data was not significant, the match was assessed to be the representative of the core state so that the further numerical sensitivity analysis could be performed.

Figure 40 and Table 7 shows the comparison between experimental data and the history matching result. Overall the simulation curve was matching to the experimental curve, even though there were slight differences in the early rates. The simulation curves show a similar trend from the experimental data.

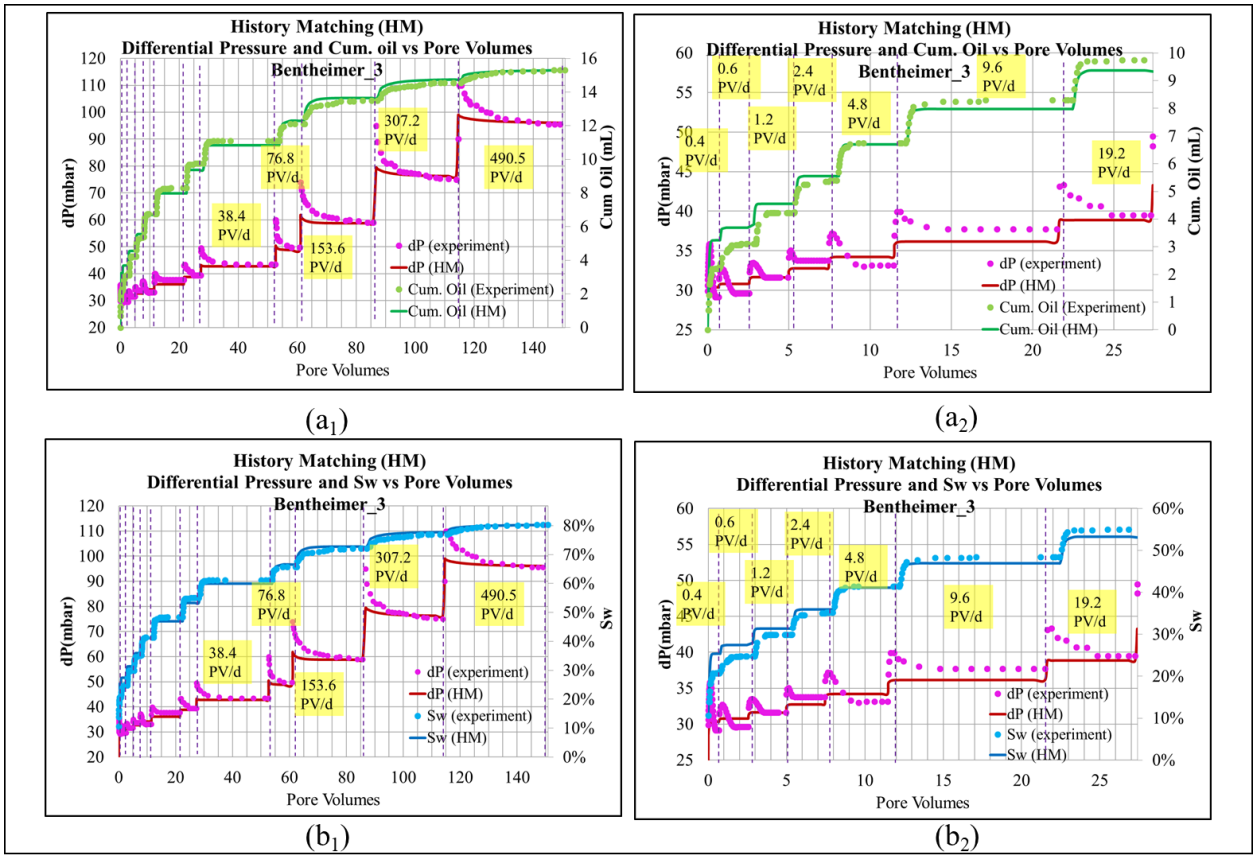

Figure 40. History Matching of Bentheimer_3 (a) Differential Pressure and cumulative oil vs Pore Volumes: (1) for all rates; (2) for earlier rates; (b) Differential Pressure and Sw vs Pore Volumes: (1) for all rates; (2) for earlier rates.

Table 7. The comparison between experimental data and history matching data on Bentheimer_3.

Rate PV/day	Rate mL/min	Injected PV	Experiment		History Matching	
			Incremental Oil (mL)	Incremental Sw	Incremental Oil (mL)	Incremental Sw
0.4	0.0061	0.7	2.2	20.7%	3.2	25.4%
0.6	0.0092	1.9	0.9	4.1%	0.5	2.1%
1.2	0.0183	2.4	1.1	5.1%	0.9	3.9%
2.4	0.0366	2.5	1.2	5.3%	1.0	4.6%
4.8	0.0733	4.0	1.4	6.1%	1.1	5.2%
9.6	0.1465	10.0	1.6	7.1%	1.3	5.8%
19.2	0.2931	5.8	1.5	6.6%	1.4	6.4%
38.4	0.5861	25.3	1.4	6.1%	1.5	6.7%
76.8	1.1723	8.3	1.0	4.5%	1.5	6.7%
153.6	2.3488	24.8	1.4	6.4%	1.4	6.1%
307.2	4.6976	28.2	1.1	4.8%	1.1	5.0%
490.5	7.5	35.1	0.8	3.4%	0.5	2.5%
Total		**149.1**	**15.3**	**80.3%**	**15.3**	**80.3%**

6.2 Sensitivity

By using the simulation curves for capillary pressure and relative permeability, sensitivity analyses were performed. The reference parameters for all the sensitivity can be seen in Table 6. Leverett scaling is not an option in SENDRA and was not applied in the sensitivity analysis.

6.2.1 The role of capillary pressure

Figure 41 and Figure 42 shows the comparison between non-zero capillary pressure and zero capillary pressure. The same experimental procedure was used regarding rates and injected PVs (Table 7). All parameters seen in Table 6 were kept constant except c_w and c_o were set to be zero. The capillary end effect is present when the system has capillary pressure, but not at the system without capillary pressure. If there is no capillary pressure, it should be no end effect and it should be similar to the water-wet case. Even though several rates were applied in the simulation, there was no rate dependency on oil production as can be seen on Figure 42 left. The differential pressure without Pc is lower compared to the system with Pc, which means with lower differential pressure, the system without Pc can produce more oil compared to the system with Pc.

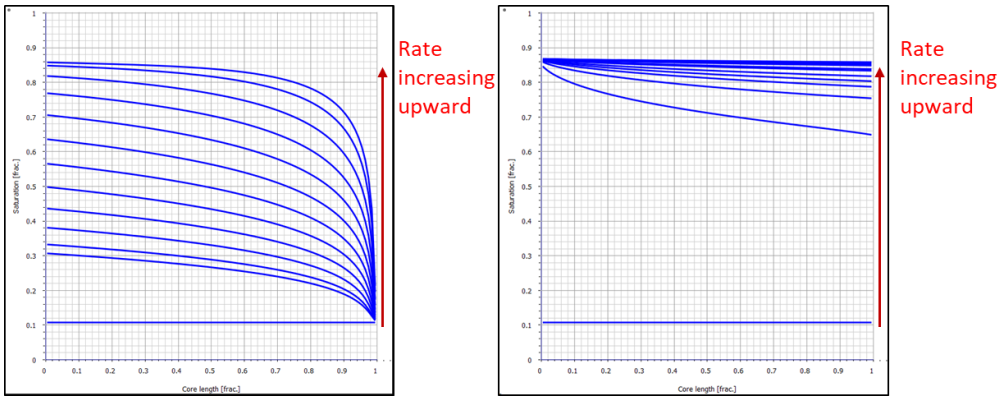

Figure 41. Saturation distribution along the core: (left) with Pc (Right) without Pc.

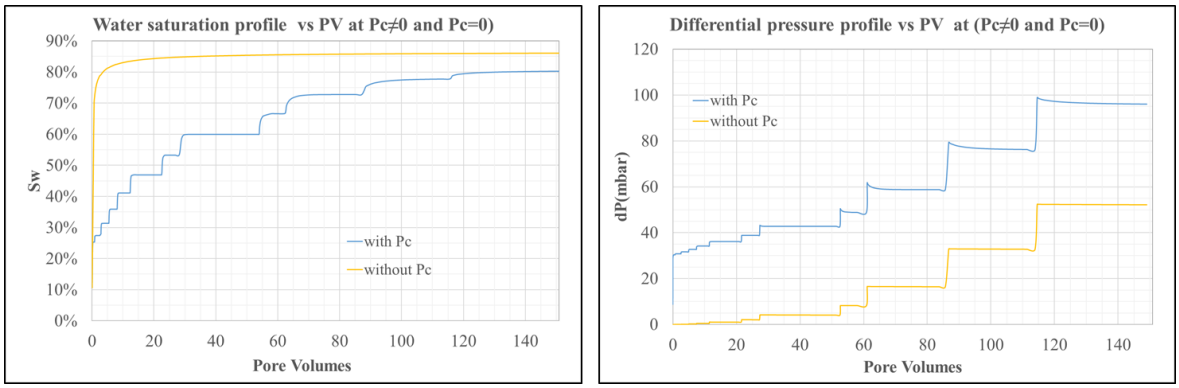

Figure 42. The comparison of water saturation profile vs PV and differential Pressure profile vs PV between with Pc and without Pc.

6.2.2 Wettability

In this sensitivity, A is the reference model from the history matching. B and C were created in SENDRA to be less oil-wet compared to A. The water saturation after spontaneous imbibition in B and C were changed due to the difference on wettability. The Corey and Skjæveland parameters were also changed to create a new relative permeability and capillary pressure curves (Figure 43). The shape of permeability curves was based on Craig (1993) who propose the following guidelines for permeability curves (Table 8).

Table 8. The guidelines of relative permeability curves based on Craig (1993)

	Water-wet	**Oil-wet**
S_{wi}	>20 to 25%	<15%, usually 10%
k_{rw} =k_{ro}	At S_w >50%	At S_w <50%
k_{rw} at S_{or}	<0.3	>0.5, approaching 1.0

While the capillary pressure curves were made based on Heiba et al. (1983). Figure 44 shows the water saturation along the core for system A, B, and C at the end of each rate. The outlet of end saturation is fixed at saturation after spontaneous imbibition and this is corresponding to Virnovsky et al. (1995). The capillary end effect is more significant on A which is more oil-wet compared to A and B. From Figure 45 left; there is a rate dependency on A and B, but not in C, since most of the oil in C is produced on spontaneous imbibition. Higher differential pressure is needed on B and C to produce more oil on forced imbibition (Figure 45 right).

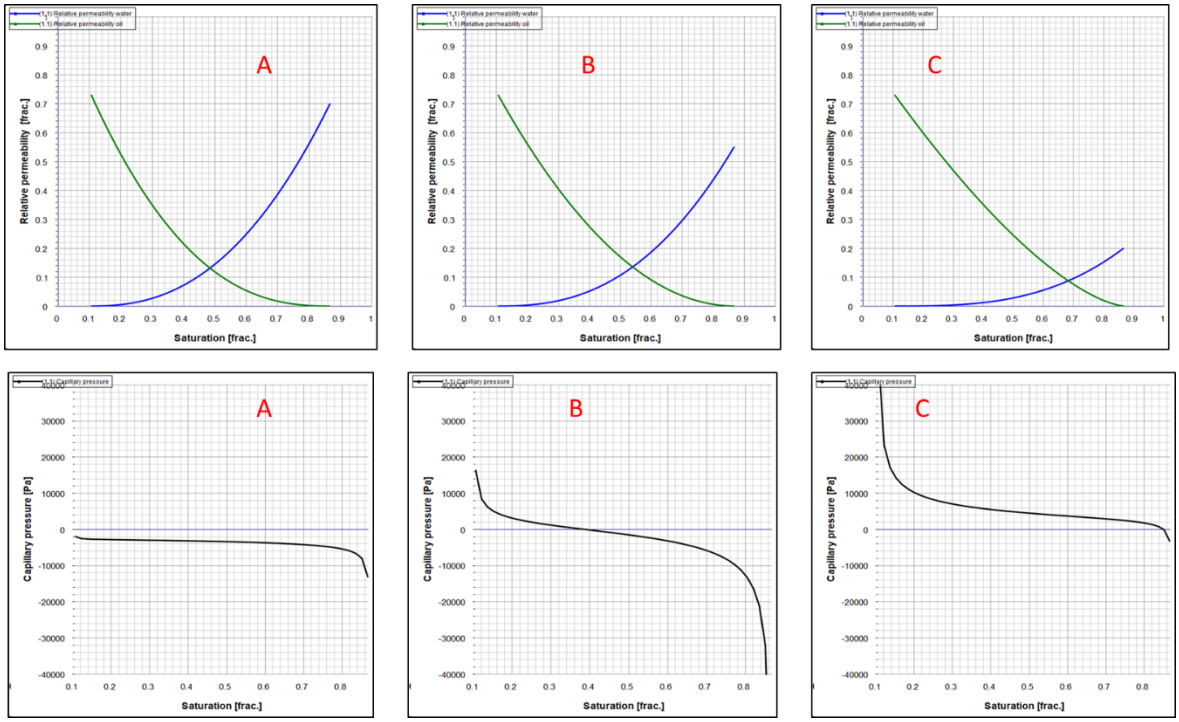

Figure 43. Relative permeability and capillary curves for A, B, and C.

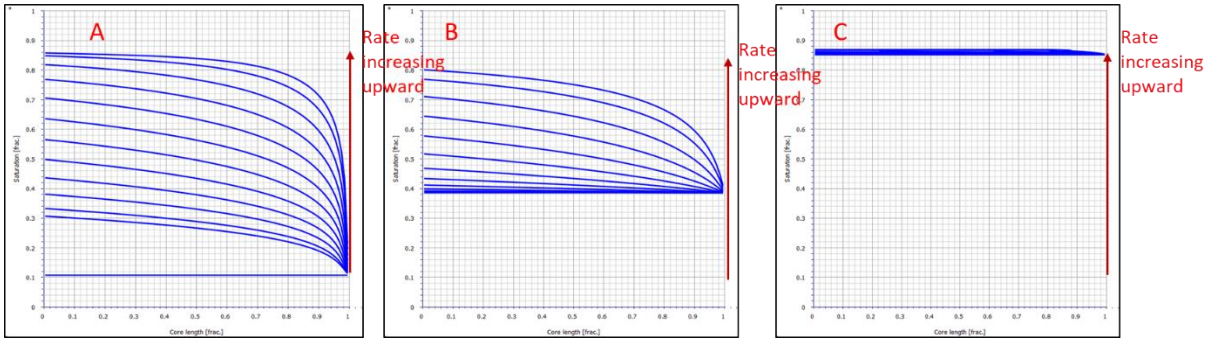

Figure 44. Saturation distribution along the core for A, B, and C.

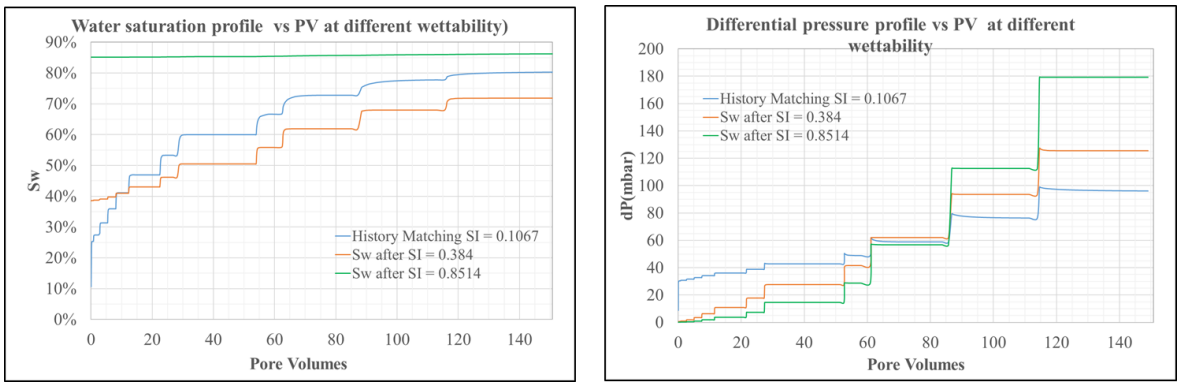

Figure 45. The comparison of water saturation profile differential Pressure profile vs PV for different types of wettability.

6.2.3 Absolute permeability

Absolute permeability reference for the sensitivity corresponds to Table 6 which is equal to 3.1 Darcy. Leverett scaling was not used in the simulation. The absolute permeability is varied at 0.1 times reference permeability (0.31 D) and 0.5 times reference permeability (1.55D). The other parameters were kept constant. The result of the simulation corresponds to equation (24) in which the capillary end effect can be minimised when the absolute permeability is low as can be seen in Figure 46 and Figure 47. However, for low permeability core, a higher pressure is needed to produce oil compared to a high permeability core especially on a higher rate (Figure 46 right), and it corresponds to Darcy's law (equation (3)).

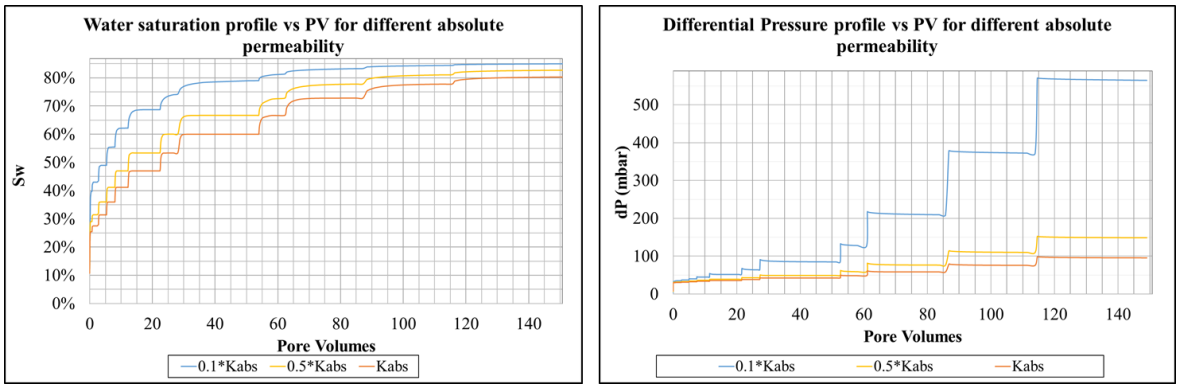

Figure 46. The comparison of water saturation profile and differential pressure profile vs PV for different absolute permeabilities.

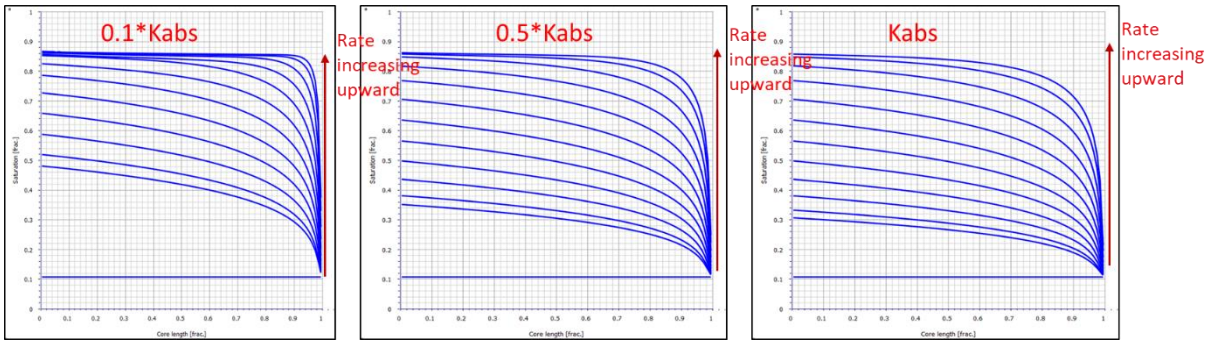

Figure 47. Saturation distribution along the core for different absolute permeabilities.

6.2.4 Rate

Rate reference for the sensitivity corresponds to Table 7. The end effect decreases as the injection rate increases (Figure 48), it corresponds to the previous study. (Hadley and Handy, 1956; Abeysinghe et al., 2012; Virnovsky et al., 1995; Rapoport and Leas, 1953). For some cases, a high rate is impractical due to the laboratory equipment capacities, and it could also damage the core because of high stress (Virnovsky et al., 1995). Figure 48 (right) shows the

increase of differential pressure on a higher rate, and it corresponds to Darcy's law (equation (3)).

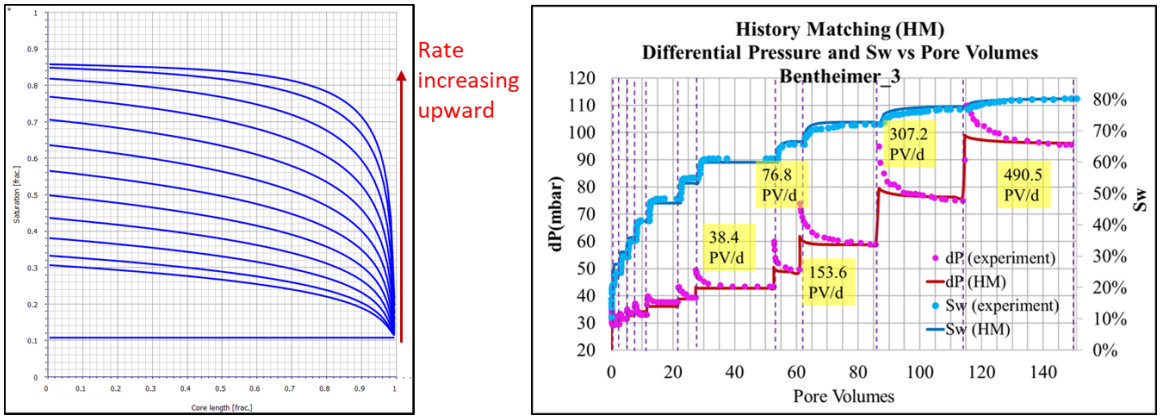

Figure 48. Left: Saturation distribution along the core; Right: The saturation profile and the differential pressure profile vs PV of Bentheimer_3

6.2.5 Viscosity of water

The viscosity of water corresponds to Table 6 which is equal to 1.09 cp. The viscosity of water has the same effect as the constant rate (equation (24)). The viscosity of water was varied at four times reference water viscosity (4.36 cp) and 10 times reference water viscosity (10.9 cp). Figure 50 shows that the capillary end effect will be less significant at higher water viscosity and it corresponds to equation (24). Figure 49 (right) shows that the higher viscosity will give the higher differential pressure, and it corresponds to Darcy's law (equation (3)).

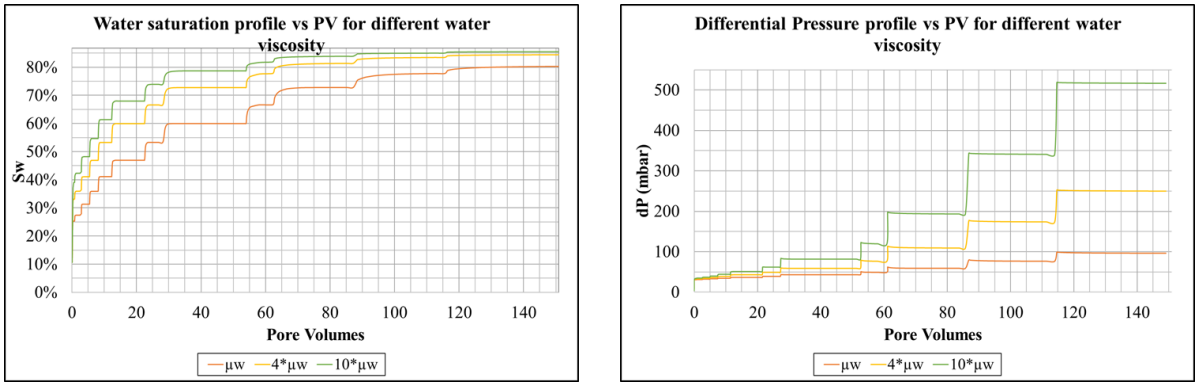

Figure 49. The comparison of water saturation profile and differential pressure profile vs PV for different water viscosities.

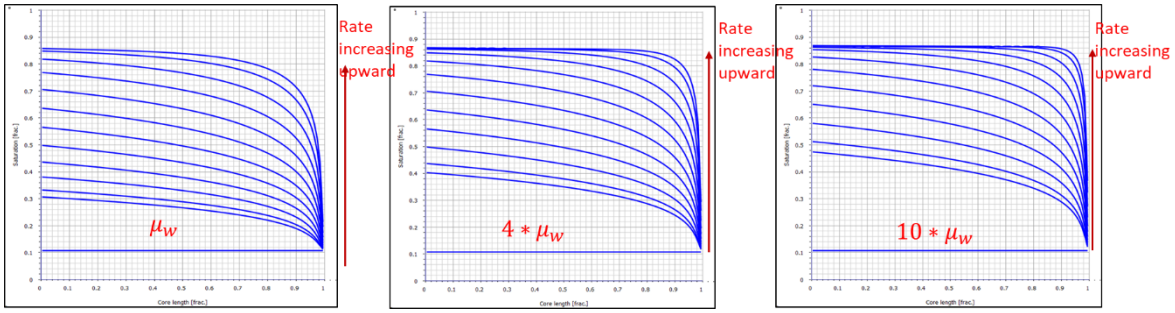

Figure 50. Saturation distribution along the core for different water viscosity.

6.2.6 Length of the core

The length of the core corresponds to Table 6 in which is equal to 90.03 mm. The amount of injected pore volumes per rates are kept constant when doing the sensitivity for the length. The length of the core was varied at four times reference length (360.12 mm) and 10 times reference length (900.03 mm). Since the pore volume is changing, then the cumulative oil production is also changing (Figure 51). The capillary end effect will be less significant on the long core (Figure 52). Equation (24) shows the similar correlation as scaling factor $Lu_T\mu_w$ from Rapoport and Leas (1953) where capillary end effect can be minimised when the rate is high, the water viscosity is high, and the length of the core is long.

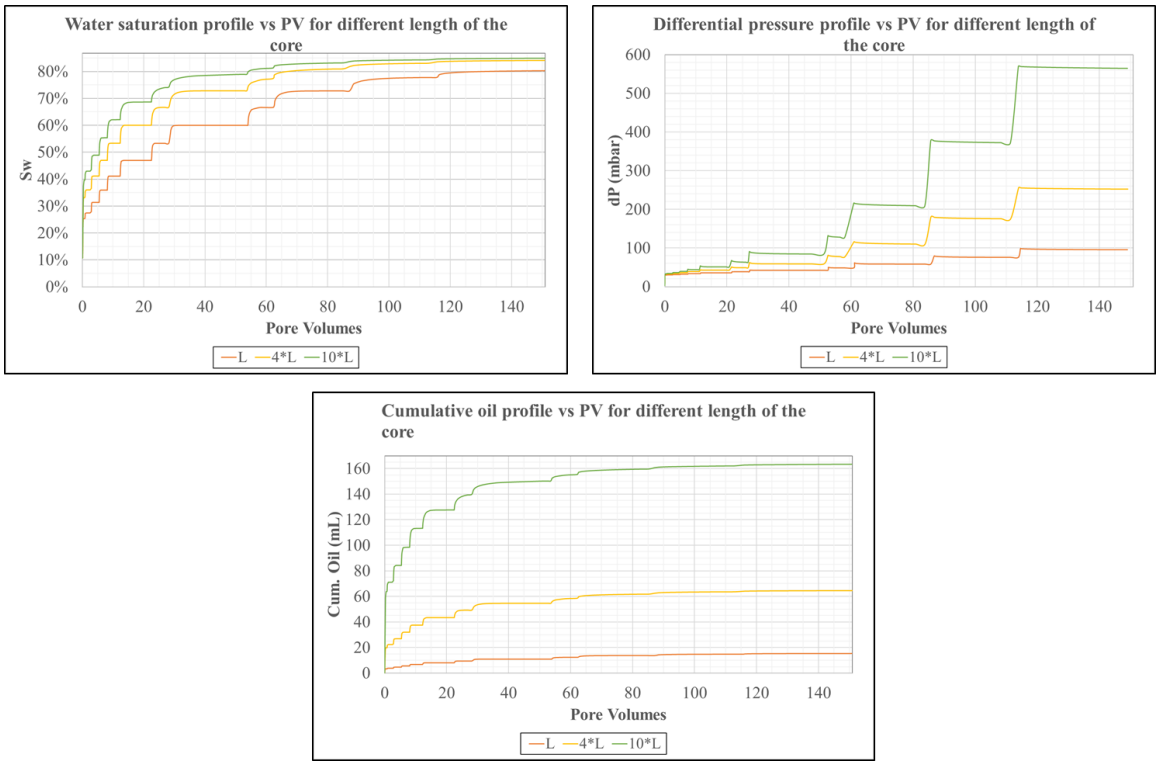

Figure 51.The comparison of water saturation profile and differential pressure profile vs PV for different lengths of the core.

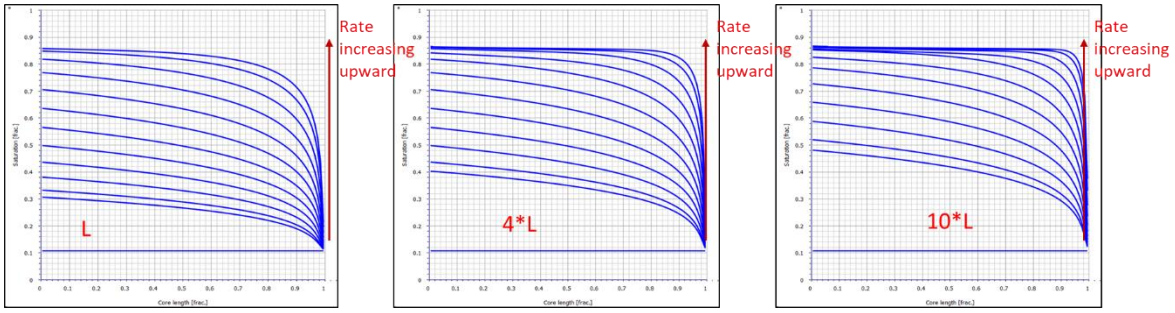

Figure 52. Saturation distribution along the core for different lengths of the core.

6.2.7 Viscosity of oil

The viscosity of oil reference for the sensitivity corresponds to Table 6 which is equal to 0.92 cp. The viscosity of oil was varied at ten times viscosity of oil reference (9.2 cp) and 40 times viscosity of oil reference (36.8 cp). The other parameters are kept constant. From Figure 53 and Figure 54, there is no significant effect of oil viscosity on the earlier rate. The water breakthrough for at the first rates is the same for all oil viscosity. However, after that, the higher oil viscosity had a longer tail production compared to the lower oil viscosity. At the higher rate, it will take more time to reach the steady state (Figure 53 left).

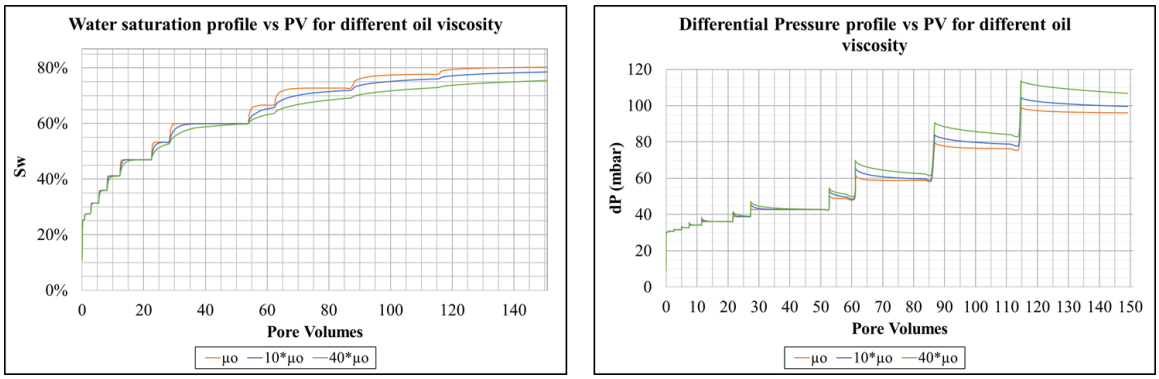

Figure 53. The comparison of water saturation profile and differential pressure profile vs PV for different oil viscosity.

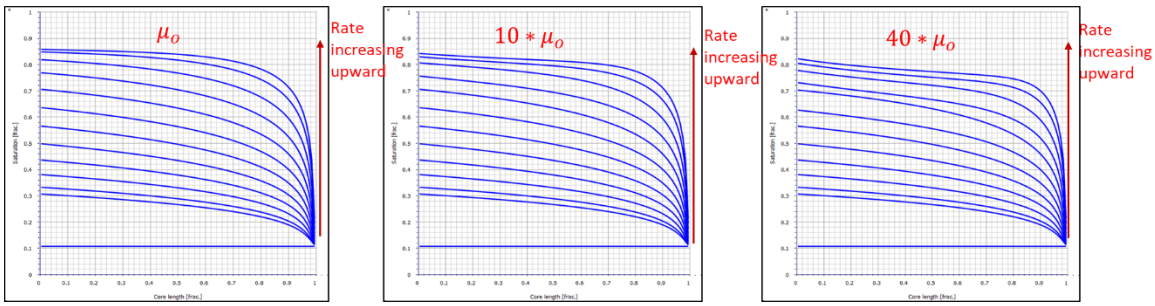

Figure 54. Saturation distribution along the core for different oil viscosity

The final saturation for imbibition procedure at high oil viscosity is less than at low oil viscosity. It corresponds to Abeysinghe et al. (2012) experiment, at high oil/water viscosity

ratio more water is needed to be injected to reach residual oil saturation after water flooding. Hadley and Handy (1956) performed two sensitivity of viscosity ratio, one by keeping water viscosity constant and the other by keeping the oil viscosity constant. They observed that the end effect decreases if the non-constant viscosity in that viscosity ratio increases, but the change of oil viscosity not too significant compared to water viscosity.

7 Conclusion and recommendations

Initially, four cores samples were planned for the experimental work in this thesis. However, the wettability alteration on Bentheimer_1 was not successfully conducted. The forced imbibition result of Berea was not reliable after losing the confining pressure. For Bentheimer_2 and Bentheimer_3, forced imbibition procedure was successfully conducted. Bentheimer_3 was chosen for the numerical study because the capillary end effect was more significant compared to the Bentheimer_2 which was more water-wet. Spontaneous imbibition was conducted to create a system where P_c=0. Water flooding was performed as forced imbibition.

Based on the results and discussion, these following points can be concluded:

- The Quilon treatment on Bentheimer_2 and Bentheimer_3 change the hydrophilic surfaces into hydrophobic. This wettability alteration only changed the relative permeability of the core, but not the absolute permeability of the core. The method could be used to determine the relative permeability and capillary pressure curves.
- Berea, Bentheimer_2 and Bentheimer 3 had capillary end effect because there was oil production on forced imbibition procedure, and there was an additional production when the rate was increased (rate dependency). The end effect was seen in all the flooded cores. The oil production on Bentheimer_2 mostly happened on spontaneous imbibition, while on Bentheimer_3 mostly happened on forced imbibition procedure. Therefore, capillary end effect was more significant on Bentheimer_3 due to more oil-wet the wettability.
- Based on sensitivity on SENDRA, the capillary end effect is significant in water-flooding for a core with these criteria:
    - More-oil wet core
    - High permeability
    - Low rate
    - Highly mobile water (low water viscosity)
    - Short length of the core

  The end effect of decreases when the viscosity of oil increases, but it is not too significant compared to the other parameters above. By increasing the viscosity of oil, it will take longer time to reach steady state.

Based on the experimental findings, below are several recommendations for future works which will be useful for studying capillary end effect in the laboratory:

- In this experiment, the wettability of Bentheimer cores was successfully changed to be more oil-wet. However, the wettability of Bentheimer_2 was relatively water-wet. Therefore, more research is needed to generate different wetting condition on Bentheimer cores. Both stable colouration and stable differential pressure should be reached on the future study. Spontaneous imbibition at the water-wet state should also be measured as a comparison.
- A bypass line is needed for the core flooding experiment to control the initial low rate. By using a bypass line, a higher rate can be applied to the core to increase the system without affecting the core.

References

Abeysinghe, K. P., Fjelde, I., & Lohne, A. (2012). Dependency of remaining oil saturation on wettability and capillary number. In *SPE Saudi Arabia Section Technical Symposium and Exhibition*. Society of Petroleum Engineers.

Ahmed, T. (2001). *Reservoir Engineering Handbook* (2nd ed.). Boston: Gulf Professional Publ.

Amott, E. (1959). Observations Relating to the Wettability of Porous Rock; Trans. AIME.

Andersen, P. Ø., Standnes, D. C., & Skjæveland, S. M. (2017). Waterflooding oil-saturated core samples-Analytical solutions for steady-state capillary end effects and correction of residual saturation. *Journal of Petroleum Science and Engineering*, *157*, 364-379.

Askarinezhad, R. (2018). *Produced water management: chemical water shutoff and disproportionate permeability reduction.* (Dissertation), University of Stavanger, Stavanger. (no. 378)

Brooks, R. H., & Corey, A. T. (1964). *Hydraulic Properties of Porous Media*. *Colorado State University, Hydro Paper*, *3*, 27.

Buckley, S. E., & Leverett, M. (1942). Mechanism of fluid displacement in sands. *Transactions of the AIME*, *146*(01), 107-116. https://doi.org/10.2118/942107-G

Churcher, P. L., French, P. R., Shaw, J. C., & Schramm, L. L. (1991, January). Rock properties of Berea sandstone, Baker dolomite, and Indiana limestone. In *SPE International Symposium on Oilfield Chemistry*. Society of Petroleum Engineers.

Craig, F. F. (1971). *The reservoir engineering aspects of waterflooding* (Vol. 3, pp. 45-47). New York, NY: HL Doherty Memorial Fund of AIME.

Criollo, S. A. (2011). *Water and surfactant flooding at different wettability conditions.* University of Stavanger, Norway,

Donaldson, E., & Alam, W. Wettability. 2008. *Houston, Texas: Gulf Publishing Company*.

Green, D. W., & Willhite, G. P. (1998). *Enhanced Oil Recovery* (Vol. SPE textbook series Volume 6). Richardson, Texas: Henry L. Doherty Memorial Fund of Society of Petroleum Engineers.

Gupta, R., & Maloney, D. R. (2016). Intercept Method--A Novel Technique To Correct Steady-State Relative Permeability Data for Capillary End Effects. *SPE Reservoir Evaluation & Engineering*, *19*(02), 316-330. https://doi.org/10.2118/171797-MS

Hadley, G. F., & Handy, L. L. (1956, January). A theoretical and experimental study of the steady state capillary end effect. In *Fall Meeting of the Petroleum Branch of AIME*. Society of Petroleum Engineers.

Heiba, A. A., Davis, H. T., & Scriven, L. E. (1983). Effect of wettability on two-phase relative permeabilities and capillary pressures. In *SPE annual technical conference and exhibition*. Society of Petroleum Engineers.

Honarpour, M., Koederitz, L., & Harvey, A. H. (1986). *Relative permeability of petroleum reservoirs*. Boca Raton, Fla: C.R.C. Press.

Huang, D. D., & Honarpour, M. M. (1998). Capillary end effects in coreflood calculations. *Journal of Petroleum Science and Engineering*, *19*(1-2), 103-117. https://doi.org/10.1016/S0920-4105(97)00040-5

Frantz Jr, J. H., Hopkins, C. W., Lancaster, D. E., & Jochen, J. E. (1993, January). Reservoir and Stimulation Evaluation of the Berea Sandstone Formation in Pike County, Kentucky. In *Low Permeability Reservoirs Symposium*. Society of Petroleum Engineers.

Kestin, J., Khalifa, H. E., & Correia, R. J. (1981). Tables of the dynamic and kinematic viscosity of aqueous NaCl solutions in the temperature range 20–150 C and the pressure range 0.1–35 MPa. *Journal of physical and chemical reference data*, *10*(1), 71-88. https://doi.org/10.1063/1.555641

Lenormand, R., Lorentzen, K., Maas, J. G., & Ruth, D. (2017). Comparison of Four Numerical Simulators for SCAL Experiments. *Petrophysics*, *58*(01), 48-56.

Maini, B. B., Ionescu, E., & Batycky, J. P. (1986). Miscible displacement of residual oil-effect of wettability on dispersion in porous media. *Journal of Canadian Petroleum Technology*, *25*(03). https://doi.org/10.2118/86-03-03

Masalmeh, S. K. (2001, January). Experimental measurements of capillary pressure and relative permeability hysteresis. In *Paper SCA 2001-23 presented at the SCA Conference, Edinburgh, Scotland, September*.

Peksa, A. E., Wolf, K. H. A., & Zitha, P. L. (2015). Bentheimer sandstone revisited for experimental purposes. *Marine and Petroleum Geology*, *67*, 701-719. https://doi.org/10.1016/j.marpetgeo.2015.06.001

PubChem Compound Database. PubChem Compound Database Retrieved 16 April 2018, from National Center for Biotechnology Information https://pubchem.ncbi.nlm.nih.gov/compound/15600

Quilon data sheet. Retrieved March 2018 http://www.zaclon.com/pdf/quilon_datasheet.pdf

Quizix QX Series. Retrieved 26 June 2018 https://www.chandlereng.com/products/reservoiranalysis/core-flow/quizix-precision-pumps/qxseries

Rapoport, L. A., & Leas, W. J. (1953). Properties of linear waterfloods. *Journal of Petroleum Technology*, *5*(05), 139-148. https://doi.org/10.2118/213-G

Salathiel, R. A. (1973). Oil recovery by surface film drainage in mixed-wettability rocks. *Journal of Petroleum Technology*, *25*(10), 1216-1224. https://doi.org/10.2118/4104-PA

Skjaeveland, S. M., Siqveland, L. M., Kjosavik, A., Hammervold, W. L., & Virnovsky, G. A. (1998, January). Capillary pressure correlation for mixed-wet reservoirs. In *SPE India Oil and Gas Conference and Exhibition*. Society of Petroleum Engineers, *3*(1), 60-67. https://doi.org/10.2118/60900-PA

Virnovsky, G. A., & Guo, Y. (1995). Relative permeability and capillary pressure concurrently determined from steady-state flow experiments. In *IOR 1995-8th European Symposium on Improved Oil Recovery*.

Tiffin, D. L., & Yellig, W. F. (1983). Effects of mobile water on multiple-contact miscible gas displacements. *Society of Petroleum Engineers Journal*, *23*(03), 447-455. https://doi.org/10.2118/10687-PA

Virnovsky, G. A., & Guo, Y. (1995). Relative permeability and capillary pressure concurrently determined from steady-state flow experiments. In *IOR 1995-8th European Symposium on Improved Oil Recovery*.